



542883
P 114

**American Science
and Engineering, Inc.**
Fort Washington
Cambridge, Massachusetts 02139
617-868-1600 Telex 921-458

30 NOVEMBER 1989

ASE-5600

FINAL REPORT:

**PLASMA PROPERTIES
OF HOT CORONAL LOOPS
UTILIZING COORDINATED SMM
AND SOLAR RESEARCH
ROCKET OBSERVATIONS**

PERIOD OF PERFORMANCE:
19 OCTOBER 1987 TO 30 NOVEMBER 1989

CONTRACT: NAS5-30141

PREPARED FOR:
NASA/GSFC
GREENBELT, MD 20771

(NASA-CR-186094) PLASMA PROPERTIES OF HOT
CORONAL LOOPS UTILIZING COORDINATED SMM AND
SOLAR RESEARCH ROCKET OBSERVATIONS Final
Report, 19 Oct. 1987 - 30 Nov. 1989
(American Science and Engineering) 68 p

N91-29937

Unclas
G3/75 0243243

Final Report

PLASMA PROPERTIES OF HOT CORONAL LOOPS UTILIZING
COORDINATED SMM AND SOLAR ROCKET OBSERVATIONS

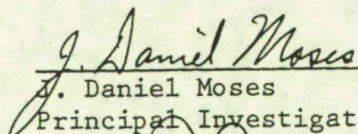
Contract: NAS5-30141

Period of
Performance: 19 October 1987 to 30 November 1989

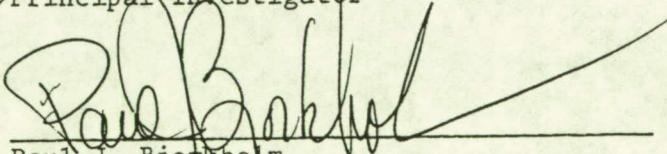
Prepared for: National Aeronautics and Space Administration
Goddard Space Flight Center
Greenbelt, Maryland 20771

Prepared by: American Science and Engineering, Inc.
Fort Washington
Cambridge, Massachusetts 02139

Approved by:



J. Daniel Moses
Principal Investigator



Paul J. Bjorkholm
Senior Vice President, Research

30 November 1989

TABLE OF CONTENTS

	<u>Page</u>
FOREWORD	i
1. INTRODUCTION	1-1
2. PROGRAM RESULTS	2-1
2.1 Background of the Program	2-1
2.2 Pre-Flight Planning and Coordination	2-2
2.3 Mission Operations and Instrument Parameters	2-5
2.4 Data Reduction and Analysis	2-9
2.5 References	2-19
3. SCIENTIFIC PRESENTATIONS AND PUBLICATIONS	3- 1
3.1 List of Presentations and Papers	3- 1
3.2 Abstracts of Presentations	3- 2
3.3 Scientific Papers	3- 3
APPENDIX A	

FOREWORD

This document is the final report for the work performed under NASA Contract NAS5-30141 and modifications 1 and 2. This work involved the pre-flight coordination, flight operations and reduction and analysis of the data obtained on solar active region 4901 on 11 December 1987 by the SMM Soft X-Ray Polychromator (XRP) and the AS&E Soft X-Ray Solar Imaging Rocket Payload Flight designated 36.038CS. The preparation, integration, and launch of the AS&E rocket payload and the initial data reduction were performed under another contract, NAS5-25496 (Final Report ASE-5568). The Contract NAS5-30141 was initially for a 1-year period of performance from 19 October 1987 to 19 October 1988, and covered per-flight planning and flight operations. Modification No. 1 extended the period of performance for a second year to 19 October 1989 and covered the reduction, analysis and initial modeling of the simultaneous SMM XRP and rocket imaging X-ray data. Modification No. 2 was for a no-cost extension to 30 November 1989, which was required to complete the analysis under the contract.

The work performed under this contract was proposed in response to NASA Space Science and Applications announcements in 1986 and 1987 for participation in the SMM Guest Investigator Program. Under the contract, AS&E was to provide improved measurements of the plasma properties of hot active region loops which would lead to advances in modeling of coronal loop magnetic confinement and energy balance. These improved measurements of loop plasma properties were to be obtained by the combination of high spectral resolution observations of an active region by the SMM Soft X-ray Polychromator (XRP) with simultaneous high spatial resolution observations of the same active region during an AS&E Solar Soft X-Ray Imaging Rocket Payload flight.

This effort was performed at AS&E under the direction of Dr. J. Daniel Moses, Principal Investigator.

1. INTRODUCTION

The overall goal of this contract was to study the magnetic confinement and energy balance of hot ($T > 10^6$ K) active region coronal loops. This was to be accomplished by comparative analysis of high spectral resolution observations of an active region by the SMM Soft X-Ray Polychromator (XRP) with simultaneous high spatial resolution broadband observations of the same active region during an AS&E Solar Soft X-Ray Imaging Rocket Payload flight. The coordination and subsequent analysis of these observations would also provide a unique opportunity for detailed examination of the assumptions required to obtain plasma parameters when each of these instruments is used alone.

The simultaneous observations necessary for this study were obtained on 11 December 1987 of active region AR 4901 by the SMM XRP and the AS&E soft X-ray rocket flight designated 36.038CS. In addition, ground-based optical, magnetogram and radio observations were also obtained in conjunction with the successful Coronal Magnetic Structures Observing Campaign (CoMStOC). Taken together, these observations provide a unique data set which is being used to study the magnetic and plasma properties of an active region.

Regarding the combined XRP and rocket X-ray data, requiring consistency between the plasma properties derived from the rocket X-ray broadband images and from the XRP X-ray line emission provides more information and accuracy about the temperature distribution of the plasma than through the use of either technique alone. The high spatial resolution images give essential information on the distribution of matter within each pixel of the high spectral resolution observations, providing a great improvement in diagnostic capability without the need to invoke ad-hoc filling-factor assumptions. Such improved measurements of the plasma properties of coronal loops will provide more stringent tests of the models of active region loop magnetic confinement and energy balance.

The preparation and launch support of the AS&E rocket payload, 36.038 CS, on 11 December 1987 was supported by NASA under a separate contract. This report summarizes only those activities directly related to the coordinated rocket and XRP observations of active region 4901. These activities are described in the

next four sub-sections under the areas of pre-flight planning and coordination, pertinent instrument descriptions, flight operations, and the reduction and analysis of the data. We emphasize that, although the analysis of the rocket image data is reasonably complete, the analysis and interpretation of the combined XRP/AS&E data set is at a preliminary stage. Section 3 lists the publications and presentations by AS&E personnel in which results pertaining to the 11 December 1987 rocket data were discussed. An abstract and a paper describing preliminary results of analysis of the X-ray data of active region 4901 appear in this section. Finally, a summary of the CoMStOC Observing Campaign is included as Appendix A.

2. PROGRAM RESULTS

2.1 Background of the Program

X-ray observations have greatly improved our knowledge of the structure of the inner corona. The identification of X-ray loops as the dominant structure of active regions has led to the realization that in order to understand the nature of the solar coronal atmosphere, it is necessary to understand the physics of the loops themselves. However, our current knowledge is very fragmentary (see Webb, 1981, for a review). Gross morphological descriptions, but few precise measurements, are available of the physical parameters within loops. This frequently leads to theoretical descriptions of loops based on assumptions, such as the formulation of the energy balance and heating function, which are not necessarily supported by observations. Comparisons between models and observations of loops are inconclusive because of the lack of high spatial resolution, multi-wavelength data and information on the three-dimensional structure of the coronal magnetic field.

Most high spectral resolution measurements in solar X-rays have been obtained with fairly broad angular resolution (Davis et al., 1975; Pye et al., 1978; Webb, 1981). These have revealed that the emission measure at a particular temperature declines steeply at high temperatures. However, some material at temperatures $> 5 \times 10^6$ K has been detected in non-flaring active regions (e.g., Schadee et al., 1983). On the other hand, broadband spectroscopy obtained with high spatial resolution X-ray images indicates a relatively narrow distribution of weighted average line-of-sight temperatures. Almost all active region loops seem to have "color" temperatures in the range 2 to 3×10^6 K. It is likely that each hot coronal loop contains a complete distribution of temperatures which is unresolved by X-ray images at the 2 to 3 arc-second level.

In the absence of spectroscopic observations with arc-second spatial resolution, one must solve this problem by modelling. The Flat Crystal Spectrometer (FCS) of the SMM XRP has better spatial resolution (15 arc-second FWHM) relative to the angular dimension of a single active region loop than any previous observations in this regime (Davis et al., 1975; Pye et al., 1978). However,

even with the improved XRP spatial resolution, the spectrometer field of view always includes a range of coronal structures at varying temperature. Therefore, any given XRP spectrum contains a distribution of emission measure with temperature. The ultimate goal of our study is to convert this into a distribution of temperature and pressure as a function of position within the loop by combining the spectroscopic distribution from the FCS data with the soft X-ray rocket images of the average distributions of temperature and pressure along the loops.

2.2 Pre-Flight Planning and Coordination

The planning of the XRP/AS&E collaboration was driven by a number of factors that were not always easily satisfied. First, the timing of the launch of AS&E's rocket payload was constrained by the timetable for collaboration in a study of small-scale coronal structures with another rocket flight conducted by the NRL HRTS group and with ground-based measurements of solar microwaves, photospheric magnetograms, He-I 10830A, H-alpha, and Ca-II K network. Second, the overall collaboration was constrained by the requirements of the CoMStOC program, which required the coordination of XRP and ground-based Very Large Array (VLA) observations of suitable active regions. Third, for the XRP/AS&E study we needed to select a suitable active region for study. Desirable qualities included a reasonably bright, hot region for the rocket CCD experiment and XRP diagnostics, but one that was fairly stable in output and positioned near the center of the Sun. For the NRL collaboration we desired the presence of several sunspot groups for coregistration of the NRL EUV and AS&E X-ray images. Active patrol of candidate regions by the XRP one or two solar rotations before the nominal launch date was desirable.

We planned to make use of two capabilities of the SMM XRP FCS experiment: (1) spectral scans between 1.4 and 22.4 A of a 15 arc-second (FWHM) square resolution element and (2) raster scans of areas up to 5 x 5 (arc-minute)² in size at the peak wavelengths of important soft X-ray lines which are diagnostic of coronal material formed between 2 and 50 x 10⁶ K.

A target active region was to be determined by discussions between the AS&E and the XRP investigation teams during the solar rotation prior to launch. Primary XRP observations would begin when the target active region transited the east limb. At regular intervals thereafter, polychromator raster scans of the hot coronal portion of the active region would be obtained by the FCS with at least daily scans continuing until the active region transited the west limb. These scans would permit us to place the rocket/XRP observation in the evolutionary context of the active region. Also, the scans obtained near the east and west limbs would help resolve ambiguities from the two-dimensional X-ray disk observations on the height and shape of the loops chosen for analysis.

On the day of the launch during a period bracketing the rocket observations, the FCS was to obtain a series of spectra at specific points within the active region, as well as raster images in specific lines of the entire active region covering as wide as possible a range of temperatures.

The first attempt at simultaneous XRP and AS&E rocket observations was scheduled for 8 June 1987, but subsequently cancelled due to a complete lack of solar activity. Active region 4811 had been observed by XRP on a nearly continuous basis during its transit as part of the coordinated observing plan and was expected to return to the east limb on 10 and 11 June 1987. The launch attempt was rescheduled for 10 June but an abort at T -2 seconds due to a failure in the boost phase guidance stage of the rocket resulted in cancellation of all launch activity until the failure could be understood. AS&E scientist K. Hester Waljeski was present at Goddard Space Flight Center during the June launch interval to provide coordination of observing efforts with the XRP team. D. Webb was at White Sands helping to coordinate the overall AS&R/NRL small-scale structure campaign.

Shortly after the 10 June 1987 launch attempt the XRP gas supply system for the low energy detectors was shut down due to critically low reserves. Since cycling the gas system was believed to shorten its life expectancy, a decision was made by the XRP investigators not to turn on the gas supply without sufficient solar activity or the prospect of a useful coordinated month-long program. When an apparent resolution was obtained to the June sounding rocket

abort, another launch attempt was scheduled for August. On 15 August the AS&E rocket (36.021 CS) was successfully launched, but the rocket flight of the NRL HRTS payload scheduled for launch immediately after 36.021 CS was aborted for reasons similar to the 10 June abort. Unfortunately, conditions were not considered sufficient by XRP investigators to turn on the low energy detector gas supply system in support of the 15 August AS&E flight.

These factors created a strong incentive to quickly recycle the AS&E payload for another launch attempt. At the same time, the XRP investigators were planning to participate in the month-long Coronal Magnetic Structures Observing Campaign (CoMStOC) planned for November and December 1987. After careful discussion of all options, the collaborators agreed that the overall objectives could best be met by a reflight of the AS&E payload, as 36.038 CS, with the NRL HRTS payload on 11 December 1987 during the CoMStOC period.

The target active region on 11 December 1987 was determined to be AR 4901 located at about S20W70. The AS&E rocket payload functioned successfully during its flight and returned excellent data. XRP observations were also successful and indicated that the region was moderately stable but bright enough for good diagnostics. The NRL rocket launch was also successful, but it was mispointed away from AR 4901. Observations were also made at the Owens Valley and VLA radio telescope facilities as well as the Big Bear, Kitt Peak, and Sacramento Peak Optical facilities. The optical observations include high resolution magnetograms, HeI 10830 A images, H-alpha images and CaK images. K. Waljeski was again present at GSFC to provide coordination and XRP operations support.

2.3 Mission Operations and Instrument Parameters

The operations for the XRP/AS&E collaboration on 11 December 1987 were determined by the combined requirements of that collaboration and those of the NRL/AS&E small-scale structure campaign and the overall CoMStOC campaign, as discussed above. These mission operation plans were developed through a series of meetings and correspondence between the AS&E investigators and the SMM XRP EOF personnel. The observing program was refined in the days leading up to the flight through the interactions with K. Waljeski and FAX and telephone updates to the AS&E team at WSMR. Particularly useful were the XRP Quint Maps of target regions. The implementation of the mission operations and the resulting observations are described below.

2.3.1 AS&E Solar Soft X-Ray High Resolution Imaging Rocket Payload

Historically, solar observations with AS&E instrumentation have been driven by the quest for increasingly higher spatial resolution of coronal structures. This requirement is in response to the need to determine the detailed plasma characteristics of coronal structures, especially loops, on sub-arc second scales to adequately constrain theoretical models. Each improvement of spatial resolution in X-ray astronomy has led to an improved understanding of high energy astrophysical processes. The spatial resolution of current solar X-ray grazing incidence telescopes is limited in part by the physical size of the telescopes with focal lengths great enough to produce plate scales matched to the spatial resolution of practical X-ray detectors.

The rocket imaging system used for both of the 1987 flights utilized two new technologies which are attempts to advance the state of the art in terms of spatial resolution, energy sensitivity and calorimetry. A grazing incidence relay optics (GIRO) system, which magnifies the image from the primary mirror, was developed at AS&E to address the spatial resolution problem. A compound mirror system utilizing a Wolter-Schwarzschild Type I primary mirror and an externally reflecting hyperboloid-hyperboloid secondary mirror was designed and tested at AS&E and flown on the 1987 flights. A CCD X-ray sensitive camera was also developed, tested and flown on these flights. Such a system has improved

temporal resolution, dynamic range and linear energy response. A CCD camera is particularly well suited for use with a GIRO system since the greatly improved X-ray sensitivity of a CCD over photographic film compensates for the reduced photon flux at the GIRO image plane, while the greater plate scale of the GIRO system compensates for the lower spatial resolution of a CCD relative to fine grain film. In addition, the facility to transmit real-time X-ray images during a rocket flight is a significant advantage of electronic detectors.

Soft X-ray photographic images viewing the full disk and limb out to $1.2 R_{\odot}$ and high sensitivity soft X-ray CCD images with a restricted field of approximately 5×5 (arc-minute)² centered on the active region of choice were obtained by the AS&E rocket payload in 1987. The telescope is equipped with a 12-inch fused quartz grazing incidence primary mirror of the Wolter-Schwarzschild aplanatic design. The primary mirror has a focal length of 144.9 cm corresponding to a plate scale of 7 microns per arc second. This uncoated fused silica mirror has been used in the AS&E solar rocket program for over a decade and has exhibited excellent quality, low-scatter performance (e.g., Davis et al., 1979). The payload also contained a Nickel coated Beryllium GIRO consisting of two hyperboloidal sections (Davis et al., 1984; Moses et al., 1986). With a net 4X magnification of the image, the secondary optic matched the plate scale of the compound telescope to the spatial resolution of the electronic CCD detector. The compound telescope with the secondary mirror in place has a focal length of 536.1 cm and a plate scale of 27.3 microns per arc sec.

The X-ray sensitive CCD camera was used at the secondary focus to provide high sensitivity images with angular resolution comparable to the best obtained at the primary focus. Broadband filters were used to provide wavelength discrimination. The CCD camera uses a back-illuminated and thinned RCA SID 53612 CCD. This is a low noise, three-phase, frame transfer device with a 30 micron square pixel size. Each pixel subtends an angle of about 1 arc sec at the secondary focus. The pixels are arranged in a 320 by 256 format. The image is down-linked in real time via telemetry. The exposure and storage time requirements of this system required a low CCD noise level which can only be accomplished with operating temperatures around -100°C . A liquid nitrogen dewar system was

developed to maintain a -100°C operating temperature for the CCD during count-down, associated holds, and the rocket flight itself.

All functions of the rocket payload were controlled by the flight computer which is based on the RCA 1806 microprocessor. The experiment sequence is entered into a NOVRAM type memory which is interpreted and carried out by the resident flight program. This system provides flexibility in making real-time changes in the experiment sequence while maintaining failsafe instrument functions. Additionally, the flight computer facilitates ground support and countdown operations by providing a computer display of the payload status indicators.

A summary of the rocket instrument parameters pertinent to the two 1987 flights is presented in Table 1. On 11 December 1987 the payload was launched at 1815 UT by a Terrier-boosted Black Brant rocket. After allowing time for stabilization and target acquisition, 370 seconds of stabilized, pointed observation time was available at an altitude greater than 100 km. The flight program consisted of two steps in the following sequence:

1. Full-disk solar photographs were taken at the primary focus with the secondary mirror out of the optical path. An appropriate range of exposures through different broadband filters were utilized by the film camera, which was positioned in the optical path during launch.
2. Magnified solar images with an approximately 4 arc min field of view were recorded at the secondary focus by the CCD camera after the secondary mirror and the film camera were moved. The field of view was centered at the brightest point of AR 4901. Table 2 lists the film exposure sequence and the CCD program for the 11 December flight.

2.3.2 SMM X-Ray Polychromator

The primary objective of the XRP is to study the physical conditions in the corona for a variety of solar phenomena. This is achieved through the use of two complementary instruments: (1) The Bent Crystal Spectrometer (BCS) contin-

uously monitors the spatially integrated (over 6 arc-min) high-temperature flux from flares. The BCS has eight bent Bragg crystal spectrometers with position-sensitive detectors, of which six were working in 1987. (2) The Flat Crystal Spectrometer (FCS) images an area of ≤ 7 arc min square in up to six spectral lines, or can make rapid scans over a wide wavelength range or at high resolution across individual line complexes.

The FCS has seven Bragg crystal spectrometers that can be scanned in wavelength over a broad spectral range. At the "home position" of the wavelength drive, each channel can monitor the emission from a prominent soft X-ray line. The FCS is sensitive to a wide range of temperature ($2 \times 10^6 \text{ K} \leq T_e \leq 7 \times 10^7 \text{ K}$) and hence can detect everything from quiet-sun features to flares. By scanning its wavelength drive, the FCS can access an even wider range of soft X-ray lines and measure Doppler broadenings and shifts. The FCS isolates specific areas in the corona for study by using its narrow collimation. For details of the XRP instrument, see Acton et al. (1980).

The BCS and the FCS S XV and Fe XXV channels are flare detectors sensitive only to high coronal temperatures. The remaining detector systems, FCS Channels 1-4, have thin-window gas flow proportional counters with finite gas supplies. Channel 2 is no longer operable. The thin window FCS detectors used on 11 December 1987 in support of the AS&E flight were Channels 1 and 3. More limited scans can also be made of specific wavelength ranges of interest for determining temperatures or line broadening.

The FCS image data are obtained at a specific crystal angle or series of angles corresponding to wavelengths near the peaks of bright resonance lines. The images are accumulated while the FCS steps across an active region in a raster pattern dwelling for about one second at each pixel. Thus, the image is a convolution of spatial and temporal information.

Within these limitations, the XRP operated successfully on 11 December and, indeed, during the entire CoMStOC period from 25 November to 20 December 1987. On 11 December the FCS was pointed at AR 4901 on all orbits except the last. Table 3 lists the XRP observing modes on 11 December orbit by orbit. Fe XVII

is the most sensitive FCS line and raster maps using this line were made over an 3-4 arc-min square area centered on AR 4901 frequently during the day to record the evolutionary history of the region. So-called Quint Maps were obtained on two orbits, including the orbit of the rocket flight beginning at 1753 UT.

Quint Maps consisted of successive raster scans of varying areas in five prominent soft X-ray lines. Table 4 lists the wavelengths and the peak electron temperatures and ranges for each of these lines as determined from the contribution function calculations of Mewe (1974). On other orbits only spectral scan data were acquired. Details on the spectroscopic data pertinent to the XRP/AS&E collaboration are discussed in the next section.

2.4 Data Reduction and Analysis

2.4.1 AS&E Rocket X-Ray Broadband Data

The photographic soft X-ray images returned by the AS&E rocket were processed and digitized using the standard procedures developed at AS&E for the Skylab and rocket programs. The flight film containing the soft X-ray images was processed together with sensitometric calibration strips in AS&E's photometric film development facility. The resulting negatives were then digitized with AS&E's PDS microdensitometer, and the resultant density arrays converted to arrays of energy flux incident in the telescope focal plane. These are equivalent to maps of solar soft X-ray surface brightness in a particular waveband defined by the properties of the telescope mirrors, filters, and film.

Figure 1 shows one of the full-disk X-ray images taken with the polypropylene filter at the primary focus. Descriptions of analyses of the full-disk data can be found in Moses and Davis (1988b), Moses et al. (1989), and Webb and Moses (1989). AR 4901 is the bright active region in the lower right portion near the southwest limb.

Figure 2 is a long exposure of AR4901 obtained with the CCD camera system through the polypropylene filter. The CCD data were recorded on magnetic tape

in a digital format. The area of this image is 4 x 4 arc-min and the pixel size is one arc-sec. Details of the testing and flight performance of the GIRO/CCD system are presented in Moses and Davis (1988a) (attached). These data have not yet been incorporated into the analysis of the film images or the spectra.

In general, we followed established procedures described in the literature (e.g., Vaiana et al., 1977; Davis and Webb, 1984) for reduction and analysis of the rocket photographic images. There were two notable exceptions made in reduction of the 1987 data: (1) An improved film development system was used, and (2) a new technique was used to derive the characteristic curve of the film required for the conversion of film density to energy. These new techniques are described in detail by Moses et al. (1988), so here we will only briefly summarize them.

The film processing requirements of the sounding rocket program were met by purchasing a microprocessor-controlled film processor manufactured by King Concept Corporation. The processor is designed around a light-tight drum into which the reel-mounted film is placed. Under microprocessor control, chemistry is introduced and evacuated on a one-shot basis, and agitation occurs through rotation of the drum. The temperature of the chemistry is maintained within 0.2 degrees centigrade by a water jacket. Particular care was taken to monitor temperature soak, avoid contamination effects, and properly mix and store solutions.

The performance of the processor was monitored through the use of the same visible light sensitometric exposures used in the Skylab effort (Haggerty et al., 1975). The calibration effort consisted of 38 test batches conducted over a three-month interval. The gamma of the D log E curve was found to vary along the length of the film within a given batch by no more than 0.030 from the mean. The variables of developer dilution, temperature, rotational agitation speed, rotational agitation direction, and development time were explored and adjusted to minimize the effects of developer depletion. Within a single roll of film, density variations of 0.03 were found between step wedges of similar orientation with respect to developer flow direction. In general,

the performance of the new processor was comparable to the Skylab machine, and excellent photometric results were obtained with the 1987 exposures.

The film characteristic curve (i.e., the relationship between the photographic density and the energy incident upon the film) must be known in order to obtain quantitative information about the properties of the coronal plasma from X-ray images. The determination of the characteristic curve is complicated by the fact that the film response is wavelength dependent and the characteristics of the incident broadband radiation are not known a priori. Therefore, the determination of the film characteristic curve must be an iterative process. The wavelength dependence of the X-ray response of the SO-212 film was estimated during the Skylab program (Simon et al., 1975). The measured wavelength response of the film and the transmission function of the telescope and filter is combined with a model of the X-ray emission of solar plasma to produce a modeled characteristic curve. This modeled curve must be compared with the photographic data from the flight because the plasma parameters are iteratively adjusted to obtain a good fit to all the plasma diagnostics of these measurements.

For the 1987 analysis we used a parameterization of the film characteristic curve that was developed by VanSpeybroeck for the Skylab data analysis; it has been found to fit experimental film characteristic curves well. The relationship between k (the slope of the characteristic curve expressed in terms of the natural logarithm of energy) and γ (the slope of the characteristic curve expressed in the logarithm base-ten of energy) is

$$\gamma = 2.3 k$$

The four parameters of the characteristic curve to be determined are D_{base} , D_{max} , a_u , and γ . D_{base} and D_{max} do not vary with wavelength, so these values can be measured in the laboratory. The other two parameters, a_u and γ , are wavelength dependent and must be determined by an iterative technique (e.g., Davis and Webb, 1988).

Instead of the traditional "scatter plot" method previously used for AS&E X-ray analyses, we used the method of Cook et al. (1988) for determining the film characteristic curve by transforming and comparing density histograms from images of differing exposures. In this method histograms of density are constructed from at least two digitized images of the same region of the sun, taken with different exposure times. One of the exposures is chosen as the base exposure, and bin-by-bin the histograms for the other exposure times are constructed from the base using the trial $D \log E$ curve obtained from a monochromatic stepwedge. These transformed histograms are compared to the actual histograms of the appropriate exposure. The parameters of the characteristic curve, a and γ , are varied iteratively to get the best match between the transformed and actual histograms. This technique was used to determine the characteristic curves for the SO-212 film for AR4901 on 11 December 1987.

Following production of the calibrated energy arrays of AR4901, we followed closely the procedure discussed by Vaiana et al. (1977) for determining the relationship between the solar coronal emission and the flux imaged by the telescope at Earth. Briefly, the total irradiance at the focal plane reduces to the equation:

$$E = \frac{A}{4\pi f^2} \int_{\lambda} N_e^2(\ell) P(\lambda, T(\ell)) \Sigma_i(\lambda) d\lambda d\ell, \quad (1)$$

where E_i is the incident energy in units of $\text{erg cm}^{-2}\text{s}^{-1}$, i denotes the filter used, $\Sigma_i(\lambda)$ is the filter function, and the integration is along the line of sight. If the plasma is isothermal, the quantity $(A/4\pi f^2)$ and the emission measure, $\int_{\lambda} N_e^2(\ell) d\ell$, are constant and the irradiance ratio in two filters, in our case polypropylene (PP) and beryllium (BE), is:

$$\frac{E_{PP}}{E_{BE}} = \frac{F_{PP}(T)}{F_{BE}(T)} = R(T) \quad (2)$$

where $F_i(T) = \int_{\lambda} P(\lambda, T) \Sigma_i(\lambda) d\lambda$ and R is a function of temperature only.

We determined $P(\lambda, T)$, the spectral distribution of solar soft X-ray emission, from a version of the Tucker and Koren (1971) theoretical spectrum. The quantity $F_i(T)$ is determined for each filter function, permitting the temperature to be determined by comparing the measured and theoretical irradiance ratios. The procedure is modified to account for the $au(T)$ dependence of the filter, so that

$$R(T) = \frac{E_{PP}}{E_{BE}} = \frac{E_{PP}^{\circ} \cdot au_{BE}(T)}{E_{BE}^{\circ} \cdot au_{PP}(T)} \quad (3)$$

and we define a new quantity, Q :

$$Q = \frac{E_{PP}^{\circ}}{E_{BE}^{\circ}} = R(T) \frac{au_{PP}(T)}{au_{BE}(T)} \quad (4)$$

or

$$Q = \frac{F_{PP}(T) \cdot au_{PP}(T)}{F_{BE}(T) \cdot au_{BE}(T)} \quad (5)$$

For a given feature Q is determined from the incident irradiance ratio and $F_i(T)$ from the theoretical filtered spectrum weighted by the appropriate $au_i(T)$ dependence. The electron temperature follows immediately from the $Q(T)$ curve. The emission measure is then derived from Equation (1) for the energy array with the PP filter after determination of the dependence of $F(T)$ on $Q(T)$ over the range of interest in the active region. Figure 3 is a comparison of E_{PP} , E_{BE} , and Q obtained for AR4901.

Table 5 presents the X-ray plasma parameters for AR4901 as averaged over two spatial areas. The first is a 5 x 5 pixel area centered on the brightest core of the region. One pixel equals about 3 arc sec at the film plane. This area was chosen for comparison of the rocket data with the area of 15 arc sec FWHM subtended by one FCS pixel. A range of T_e is given because the central brightest areas on the PP and BE images were not identical. The other average was taken over a larger, approximate 7 x 7, pixel (21 x 21 arc sec) area. The

values of T_e and emission measure are similar for these two areas and consistent with previous values derived for active region plasmas. Both line of sight and volume emission measures were determined; these are lower limits since the incident energy arrays have not yet been deconvolved to remove the effects of scattering of the grazing incidence mirror. However, the primary silica mirror used on these flights has been demonstrated to have low scatter properties (Davis *et al.*, 1979), and deconvolution would probably increase the emission measure by $< 30\%$. The temperature would be unaffected by deconvolution because the scattering is to first order wavelength independent.

2.4.2 SMM XRP Spectroscopic Analysis and Comparison with Broadband Results

The analysis of the XRP FCS data on AR4901 is still in a preliminary stage. We will discuss some preliminary results which can be compared with the broadband rocket data, and outline the plan for completing the XRP/AS&E analysis and publishing the results.

In Section 2.3.2 we described the XRP instrument and the general observations obtained of AR4901 on 11 December. The observations most pertinent to this collaboration were obtained with the Quint Map sequence on the SMM daylight orbit which started at 1753 UT and continued through the duration of the rocket flight (Table 3). Seven useful raster maps were produced during this orbit in the lines shown in Table 4.

For the collaboration it is necessary to establish the evolutionary history of AR4901. An indication of its level of activity is shown in Figure 4, a plot of the GOES-6 whole-sun soft X-ray flux on 11-12 December. The time of the SMM orbit of the rocket flight is marked. This orbit occurred during a relatively quiet period following a long-duration X-ray flare in AR4901 with a peak flux of C1 at about 1400 UT. The small flare following this period at about 1930 UT, as well as the other larger flares were not reported optically and were likely associated with other east and west limb regions.

Figures 5-7 show the three FCS raster maps obtained during the rocket orbit that had the highest counting rates in AR4901. The two FeXVII maps were taken

30 minutes apart before and after the rocket flight, and show an increase of the maximum counting rate of a factor of two between these times. The other map was obtained in NeIX at 1815 UT. These images can be directly compared with the digitized broadband images in Figure 3.

XRP raster maps in the sensitive FeXVII resonance line at 15 A were obtained throughout the day to examine the variability of AR4901. This line has a fairly broad temperature response peaking at about 5 million K, and is the most sensitive active region line available. Each of the 4 x 4 arc min images is built up during a raster which takes about 10 min, so that up to six images can be obtained in the 60 min daylight portion of the 90 min SMM orbit.

The Quint map sequences consisted of maps at the peaks of various bright resonance lines, used to determine plasma parameters across the region, interspersed with wavelength scans of the brightest X-ray portion of an active region where there were sufficient counts for spectroscopy. The sequences are begun with 4 arc min maps to locate the brightest site in the sensitive FeXVII resonance line. On the 1753 UT orbit, the FeXVII maps were obtained at the start and end; in between maps were obtained in the OVIII, MgXI, NeIX and FeXVIII lines. Line profiles in each line were scanned at the brightest FeXVII point. After the initial 4 x 4 arc min FeXVII map, subsequent maps were 3 x 3 arc min, except that the hot Fe XVIII line was mapped only over a 2 x 2 arc min area to save time. A complete sequence of the five maps takes about 30 minutes. This is the most general sequence for determining plasma parameters such as electron temperature, emission measure and (unit filling factor) density across an active region from different line ratios. Only the OVIII and MgXI data are gathered at the same time, so the active region must be quiescent while successive images are made for straightforward use of line ratios.

A typical line scan over the FeXVII line at 15 A is shown in Figure 8. This scan was performed over the brightest FeVII pixel in the region. Such scans are used to get total line fluxes to determine emissivities and temperature diagnostics and for line broadening calculations.

For the moderate fluxes of AR4901, the only available temperature diagnostic was from the ratio of emissivities in the available lines. The limitations of this method arise from the uncertain atomic physics calculations, from calibration uncertainties from different ion species, especially from the solar abundance determinations. Figure 9 shows the calculated, model-dependent FeXVIII/FeXVII line ratio for the FCS. This is the best line ratio temperature diagnostic, because abundance errors are minimized and the signal to noise in each line is high.

Non-thermal X-ray line broadening in quiescent active regions has previously been observed with the XRP (Saba and Strong, 1986; Acton *et al.*, 1981). This line broadening is attributed to plasma turbulence and is important to the dynamics and heating in active region loops. Data pertinent to this question was obtained in the center of AR4901 on the orbit following the rocket flight. This program, called "AR Velocities" in Table 3, uses line profiles for four bright resonance lines - OVIII, NeIX, FeXVII, MgXI - scanned at each 10 arc sec square pixel in a 1 arc min or 30 arc sec square map around the brightest FeXVII site. Electron temperatures are determined from line ratios. The "excess line widths" above the thermal electron Doppler values can then be used to estimate velocities from turbulent motions. The data for this program have not yet been analyzed.

The plasma parameters that have been derived to date from the FCS data for AR4901 are presented in Table 6. Electron temperatures from the line ratios shown in the table were determined over two spatial regions. One was at the brightest 15 arc sec pixel (B.P.) in the center of the active region, and the other was over a 4 x 5 pixel (60 x 75 arc sec) area centered on the brightest pixel. The volume emission measure value was also averaged over this latter area.

This method of deriving temperatures makes the assumption that each region is isothermal and that the emission lines are thermally broadened only. From the Table we can see that the effective temperatures determined by the line ratios of given sets of ions is the same for all areas chosen in the FeXVIII bright region to within the uncertainties due to counting statistics. But the

temperatures measured by different line ratios are not consistent with one another. While the Fe and O ratios give a consistent temperature of about $3.2 - 3.4 \times 10^6\text{K}$, the ratios involving Ne and Mg do not indicate a consistent temperature. This is probably related to uncertainties in the solar elemental abundance determinations of Ne and Mg, as has been discussed by Waljeski et al., 1988.

These averaged plasma parameters can be directly compared with those in Table 5 derived from the rocket broadband measurements. As with previous results comparing broadband and spectroscopic data (e.g., Davis et al., 1975; Pye et al., 1978; Webb, 1981), the broadband "color" temperature is significantly lower than that derived from the spectral data. The XRP Fe and O emission measures for AR4901 are consistent at 10^{48} cm^{-3} , which is over two orders of magnitude greater than the values derived from the broadband data. The XRP value is also much higher than the values of 10^{45-47} obtained for typical active regions with Skylab EUV and X-ray data (Pye et al., 1978; Davis et al., 1975; Levine and Pye, 1980).

The reasons for this discrepancy are not yet known and must await further detailed analysis of AS&E and XRP data sets. Travel was arranged for K. Waljeski to meet with K. Strong at Lockheed Palo Alto Research Laboratories to address the plasma parameter discrepancy before the writing of this report, but the October earthquake disrupted operations at LPARL and forced the cancellation of the trip. K. Waljeski will continue to pursue this work as a thesis topic under the NASA GSRP (NGT 50308). This involvement and eventual transfer was outlined in the AS&E response to NRA-87-OSSA-12 (ASE-5357) which led to the first contract modification to NAS5-30141 (although the NASA GSRP award was still pending at the time of the submittal). The specific description of the transfer of the required data products and associated supporting documentation was included in the 8 November 1989 letter to Dr. Bohlin (DM-89-L-205) on the conclusion of the AS&E suborbital program contract NAS5-31619. Following the conclusion of the research effort of NAS5-31619, work will be continued with computer support from the NASA SMM Data Facility in Greenbelt, MD, and assistance from D. Moses and the staff at the Naval Research Laboratory. The

combined imaging and spectroscopic data sets will be used to study the plasma structure and distributions of AR4901 in the following manner.

The spectroscopic measurements will be inverted to provide an approximation to the distribution of emission measure with temperature along the line of sight. The spatial resolution of the FCS by itself is not adequate to distinguish loop structures even though the X-ray spectrometer has moderately high spatial resolution. Consequently, the conversion of an emission measure-temperature distribution from the FCS to a loop model requires additional information on the spatial distribution of the emission within its resolution element.

Beyond complementing the spatial resolution of the XRP spectroscopic observations, the broadband rocket images also provide "color" plasma temperatures which remove the mathematical difficulties in the inversion of coronal line spectra to obtain emission measures. Davis et al. (1975) established that the requirement of consistency between the spectroscopic emission measure distribution and the broadband average temperature is an adequate condition to choose between candidate solutions to the inversion of the spectroscopic data.

The procedure involves determining the appropriate form of the emission measure-temperature function $Y(T)$, using the different dependencies of the X-ray images and spectra. The broadband images are spatially resolved, but the flux is integrated over temperature. The spectra separate temperature regimes, but they integrate over space due to the coarse resolution.

The radial variation of the plasma from the X-ray images will be combined to generate data equivalent to the input spectra and images. A successful model is one in which the output and input converge within experimental and computational errors. Several loop models will be used in the fitting procedure. We will also examine the question of elemental abundances by using the two data sets to compare the accuracy of different sets of abundances.

Finally, if the XRP velocity data are adequate, we will study the sites of any Doppler-shifted material detected with the XRP velocity program with the structure observed in the broadband images. Specifically, comparison of the imaging

and the spectral observations will provide a good test of the tentative identification of the tops of loops as the site of loop heating.

The initial results from this collaboration will be reported in a paper by Waljeski et al. which is currently in preparation. Other results will be presented at scientific meetings and/or published in the literature as appropriate.

2.5 References

- Acton et al.: Astrophys. J. 224, L137, 1981.
- Acton, L.W. and 23 other authors: The Soft X-Ray Polychromator for the Solar Maximum Mission, Solar Phys. 65, 53, 1980.
- Cook, J.W., Edwing, J.A., and Sutton, C.S.: Determination of Film Characteristic Curves from Density Histograms, Publ. Astro. Soc. of the Pacific 100, 402, 1988.
- Davis, J.M., Chase, R.C., Silk, J.K., and Krieger, A.S.: The Design and Evaluation of Grazing Incidence Relay Optics, Nucl. Instrum. Methods 221, 20, 1984.
- Davis, J.M. and Webb, D.F.: A Study of the Cyclical Variations of Coronal Holes and Their Relation to Open Magnetic Fields, AFGL-TR-85-0003, 1984.
- Davis, J.M., Krieger, A.S., Silk, J.K., and Chase, R.C.: Quest for Ultrahigh Resolution in X-Ray Optics, SPIE 184, 1979.
- Davis, J.M., Gerassimenko, M., and Krieger, A.S.: The Interpretation of Simultaneous Soft X-Ray Spectroscopic and Imaging Observations of an Active Region, Solar Phys. 45, 393, 1975.
- Levine, R.H. and Pye, J.P.: Solar Phys. 66, 39, 1980.
- Mewe, R.: Calculated Solar X-Radiation from 1 to 60 A, Solar Phys. 22, 459, 1974.
- Moses, J.D., Krieger, A.S., and Davis, J.M.: The Measured Performance of a Grazing Incidence Relay Optics Telescope for Solar X-Ray Astronomy, SPIE 691, 1986.
- Pye, J.P., Evans, K.D., Hutcheon, R.J., Gerassimenko, M., Davis, J.M., Krieger, A.S., and Vesecky, J.F.: The Structure of the X-Ray Bright Corona above Active Region McMath 12628 and Derived Implications for the Description of Equilibria in the Solar Atmosphere, Astron. Astrophys. 65, 123, 1978.

- Saba, J.L.R. and Strong, K.T.: Evidence for Coronal Turbulence in a Quiescent Active Region Loop, Advances in Space Research, 1986.
- Schadee, A., DeJager, C., and Svestka, Z.: Enhanced X-Ray Emission above 3.5 keV in Active Regions in the Absence of Flares, Solar Phys. 89, 287, 1983.
- Simon, R. et al.: Response of Photographic Film to Soft X-Ray Radiation, AS&E Document ASE-3775, 1975.
- Tucker, W.H. and Koren, M.: Radiation from a High-Temperature, Low-Density Plasmas: The X-Ray Spectrum of the Solar Corona, Astrophys. J. 168, 283, 1971.
- Vaiana, G.S., VanSpeybroeck, L., Zombeck, M.V., Krieger, A.S., Silk, J.K., and Timothy, A.: The S-054 X-Ray Telescope Experiment on Skylab, Space Sci. Instrum. 3, 19, 1977.
- Vaiana, G.S., Krieger, A.S., and Timothy, A.F.: Identification and Analysis of Structures in the Corona from X-Ray Photography, Solar Phys. 32, 81, 1973.
- Webb, D.F. and Davis, J.M.: The Cyclical Variation of Energy Flux and Photospheric Magnetic Field Strength from Coronal Holes, Solar Phys. 102, 177, 1985.
- Webb, D.F.: Active Region Structures in the Transition Region and Corona, The Skylab Solar Workshop Monogram on Active Regions, F.Q. Orrall, editor, 1981.

Table 1

INSTRUMENT PARAMETERS FOR AS&E ROCKET FLIGHTS 36.021 CS AND 36.038 CS

Wavelength Range	8 - 60 A
Field of View	Film Detector: 60 x 60 (arc minutes) ² CCD Detector: 2 x 2 (arc minutes) ²
Sensor	Grazing Incidence Mirror
Detector	Photographic Emulsion (SO-212) X-Ray Sensitive CCD Camera
Spatial Resolution	Mirror 1 arc sec Film 1 arc sec CCD 2 arc sec
Spectral Resolution	Broadband Filters (1% levels): Polypropylene 8-39, 44-60 A Beryllium (13 m) 8-20 A
Temporal Resolution	Film: Bright objects, e.g. active regions: 2 sec Faint objects, general corona: 10-200 sec CCD: Bright objects: 0.25 sec

Table 2

AS&E ROCKET (36.038 CS) OBSERVING PROGRAM ON 11 DECEMBER 1987

Film Sequence: Start 18:16:38 UT, Stop 18:19:28 UT

Filter Numbers: 1: 25.4 um Be, 2: 1 um Polypropylene, 3: 1 um Polypropylene,
4: 12.7 um Be, 5: white light sunspot filter

<u>Exposure No.</u>	<u>Filter No.</u>	<u>Exposure Time (sec.)</u>
1	2	2
2	2	2
3	2	2
4	2	2
5	2	2
6	2	2
7	4	9
8	2	9
9	4	3
10	2	3
11	4	1
12	2	1
13	4	1/2
14	2	1/2
15	4	30
16	2	30
17	5	1
18	1	1/4
19	1	1/4
20	1	1/4
21	1	1/4
22	1	1/4
23	1	1/4
24	1	1/4
25	1	1/4
26	5	1
27	3	60
28	1	1/4
29	1	1/4
30	1	1/4
31	1	1/4

CCD Program: Start 18:22:05 UT, Stop 18:22:54 UT

<u>Filter</u>	<u>Exposure Time (sec)</u>
1 um Polypropylene	4
1 um Polypropylene	1
12.7 um Be & 1 um Polypropylene	8
1 um Polypropylene	1/4

Table 3

XRP OBSERVING SEQUENCE ON 11 DECEMBER 1987

<u>SMM Daylight Orbit Time (UT)</u>	<u>Observing Mode</u>
03:45 - 04:47	AR Atlases
05:19 - 06:21	Fe XVII Map
06:53 - 07:56	Fe XVII Map
08:27 - 09:30	AR Atlases
10:01 - 11:04	Fe XVII Map
11:36 - 12:38	Fe XVII Map
13:10 - 14:12 (Start of VLA Observations)	2 Quint Maps
14:44 - 15:46	Fe XVII Map
16:18 - 17:21	UVSP Alignment
18:16 - 18:20	(AS&E X-Ray Exposures)
17:53 - 18:55	"Quint" Map
19:27 - 20:29	AR Velocities
21:01 - 22:03	Fe XVII Map
22:35 - 23:37 (End of VLA Observations)	Fe XVII Map
01:07 - 01:30	AR Scan
01:44 - 02:46	Full Disk Raster Start (30% completion)

Table 4

XRP "QUINT" MAP RASTER SCAN PARAMETERS

<u>Ion</u>	<u>(A)</u>	<u>Peak T (10⁶ K)</u>	<u>Range of T (10⁶ k)</u>
O VIII	18.97	3	2-5
Fe XVII	15.01	5	3-8
Fe XVIII	14.22	7	5-8
Ne IX	13.44	4	3-5
Mg XI	9.17	6	4-9

Temperature values are determined from G(T) functions calculated by Mewe (1974).

Table 5

AR 4901 PLASMA PARAMETERS DERIVED FROM X-RAY BROADBAND IMAGES

	Deposited Energy ($\text{erg cm}^{-2} \text{s}^{-1}$)	T_e (10^6 K)	$\int N_e^2 d\Omega$ (10^{29} cm^{-5})	$\int N_e^2 dV$ (10^{45} cm^{-3})
Central Core	21.6	2.7 - 2.9	> 1.6	> 6.5
Active Region Average	18.9	2.8	> 1.3	> 5.5

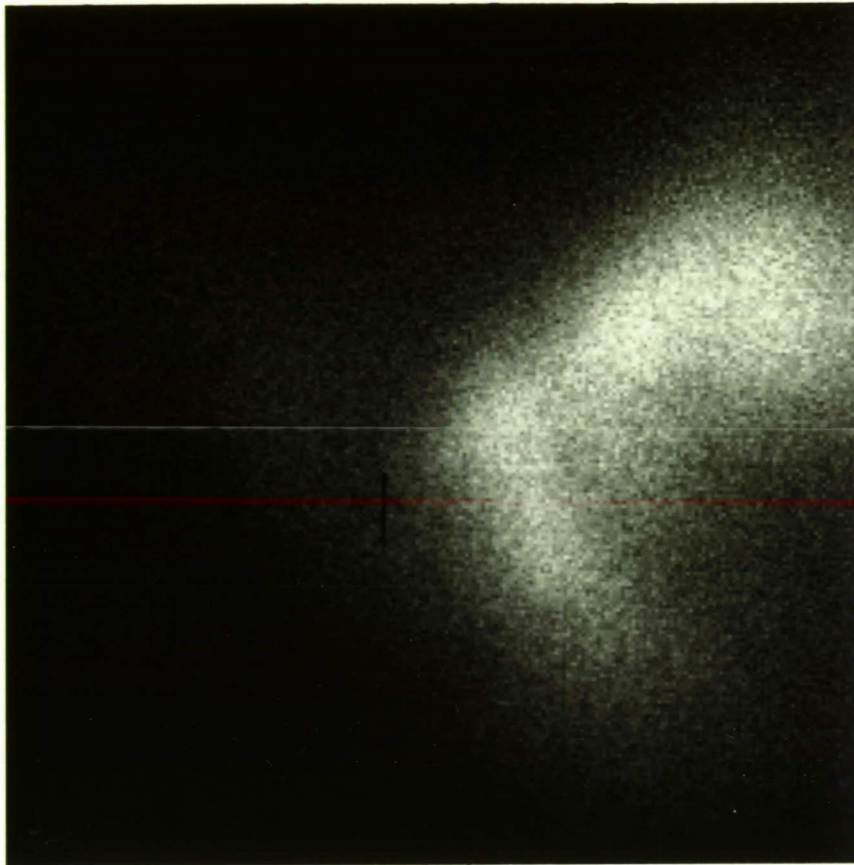
Table 6

AR 4901 PLASMA PARAMETERS DERIVED FROM XRP SPECTROSCOPIC DATA

<u>Ion Ratio</u>	<u>B.P. T(10⁶K)</u>	<u>Average T (10⁶ K)</u>	<u>Average EM (10⁴⁸ cm⁻³)</u>
Fe XVII / Fe XVIII	3.3 - 3.5	3.4	1.04
Fe XVII / O VIII	2.6 - 3.2	3.4	1.01
Fe XVIII / O VIII	3.2 - 3.4	3.4	1.00
Fe XVII / Ne IX	--	2.2	5.45
Fe XVII / Mg XI	4.8 - 5.3	4.8	1.03
Ne IX / O VIII	--	4.9	1.76
O VIII / Mg IX	3.8 - 4.3	4.3	1.31
Ne IX / Fe XVIII	3.0 - 3.2	3.1	1.79
Mg XI / Fe XVIII	2.2 - 2.9	2.5	12.71
Ne IX / Mg XI	3.8 - 4.4	4.1	1.47

Figures 1. Full disk soft X-ray image of the solar corona on 11 December 1987 (waveband 8-39, 44-60 Angstroms). Solar north is oriented up. The target region - AR4901 - is on the south west limb.

Figure 2. Soft X-ray CCD image of AR4901. The image size is 4 arc min x 4 arc min. The image was formed utilizing a 3.8X grazing incidence magnifying optic. The effective field of view is approximately 2 arc min x 2 arc min due to vignetting and geometric optical aberrations. Exposure time is 1 second through organic filters.



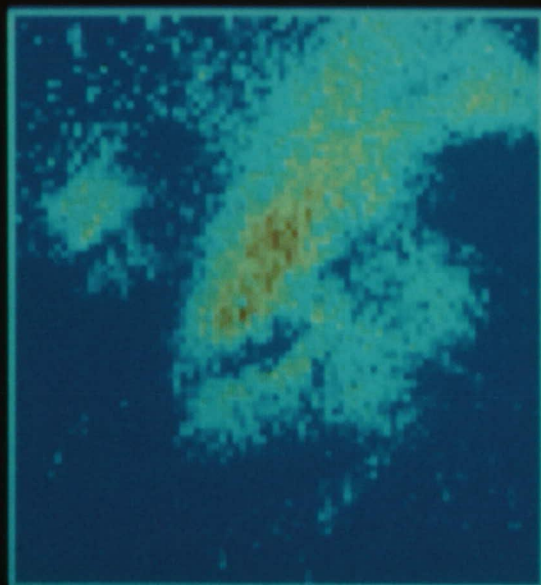
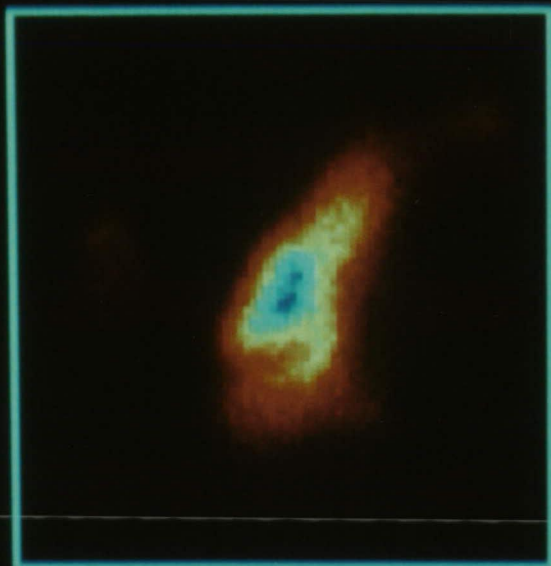
ORIGINAL PAGE
BLACK AND WHITE PHOTOGRAPH

Figure 3. Data reduction of AR4901 photographic images. Solar north is up. Field of view is 4 arc min x 4 arc min.

Top: Pseudocolor image of energy deposit in focal plane through polypropylene filter (E_{pp}). The waveband is 8-39, 44-60 Angstroms.

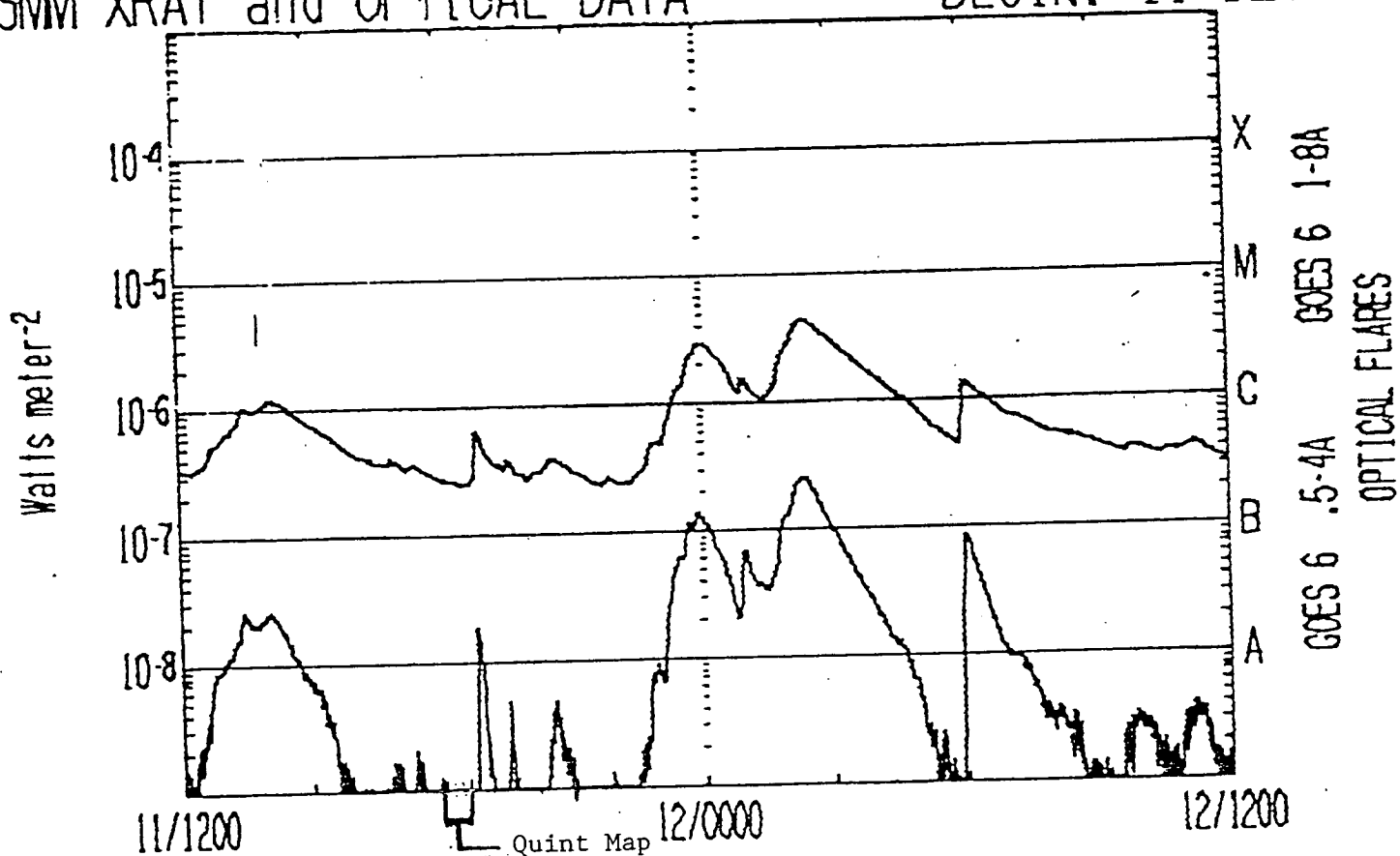
Middle: Pseudocolor image of energy deposit in focal plane through Beryllium filter (E_{BE}). The waveband is 8-20 Angstroms.

Bottom: Pseudocolor image of the electron temperature map as represented by the ratio of the two incident irradiances shown above ($Q(T)$).



SMM XRAY and OPTICAL DATA

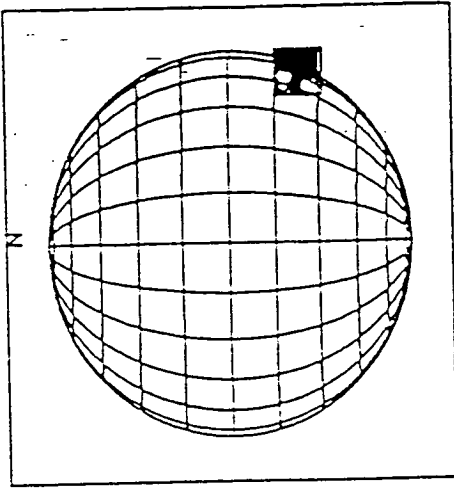
BEGIN: 11 DEC 8



SAA's
NIGHT

GOES-6 1 MIN DATA; OPTICAL FLARE DUR, IMP. REGION

Figure 4



XRP IMAGE (1st)

FCS Channel 1: Fe XVII

T: 87/345 17:55:51

Latitude: -22.13

Longitude: 72.71

Max cps = 80

Levels: 6, 7, 10, 15, 20, ..., 700

AR 4901 - Fe XVII

during rocket orbit

quint map

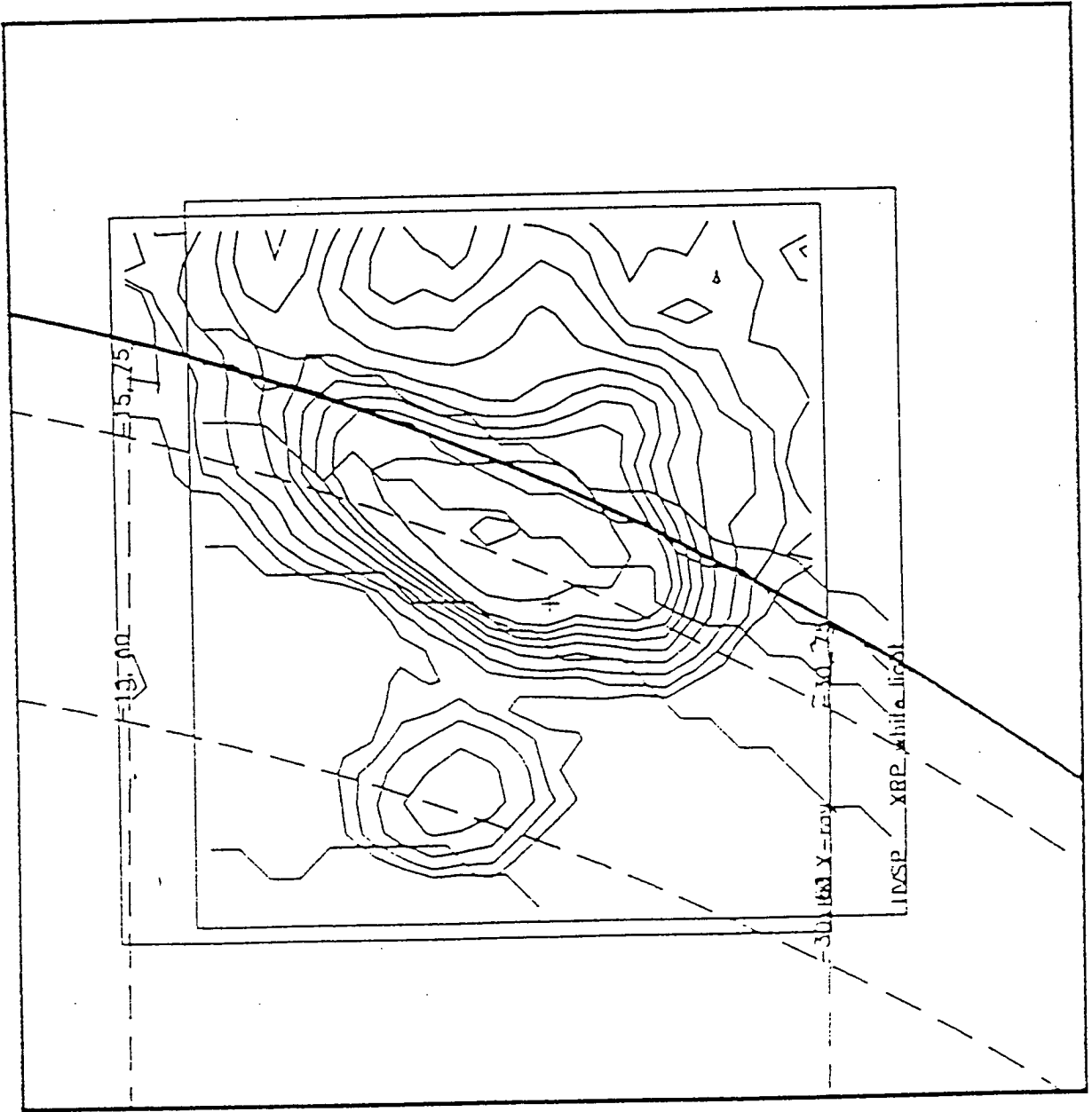
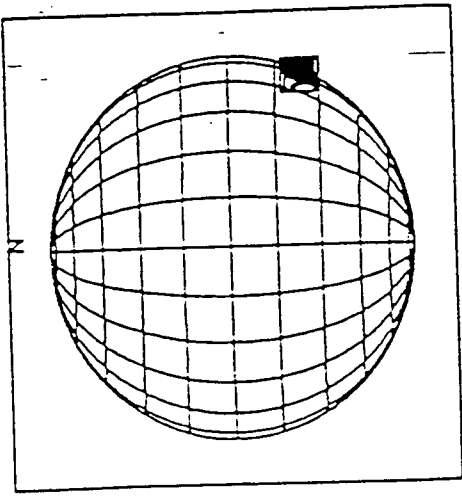


Figure 5



XRP IMAGE (2nd)

FCS Channel 1: Fe XVII

T: 87/345 18:24:37

Latitude: -22.43

Longitude: 74.50

Max cps = 155

Levels: 5,7,10,15,20,...,700

AR 4901 in nested orbit

Quiet map

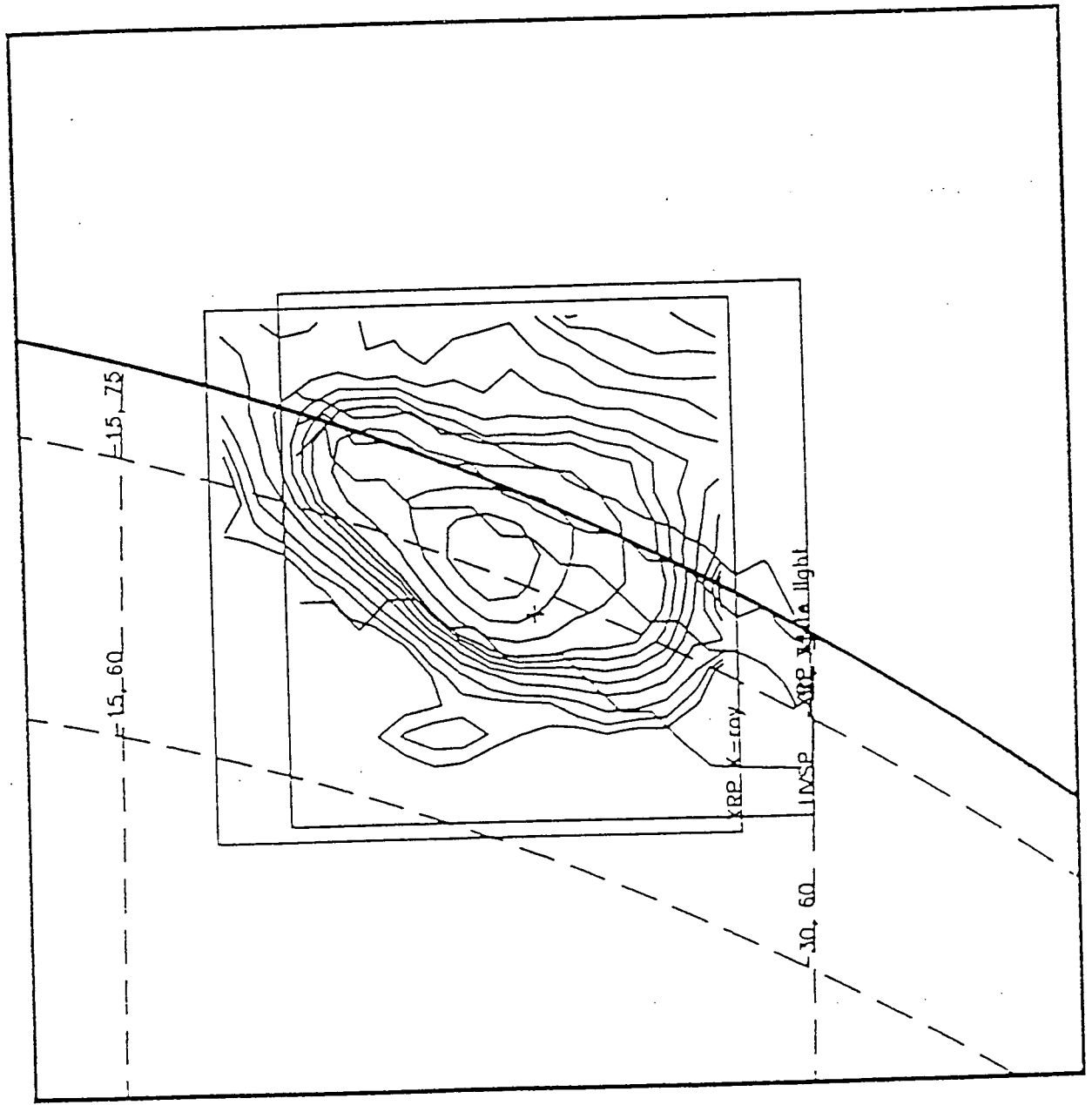
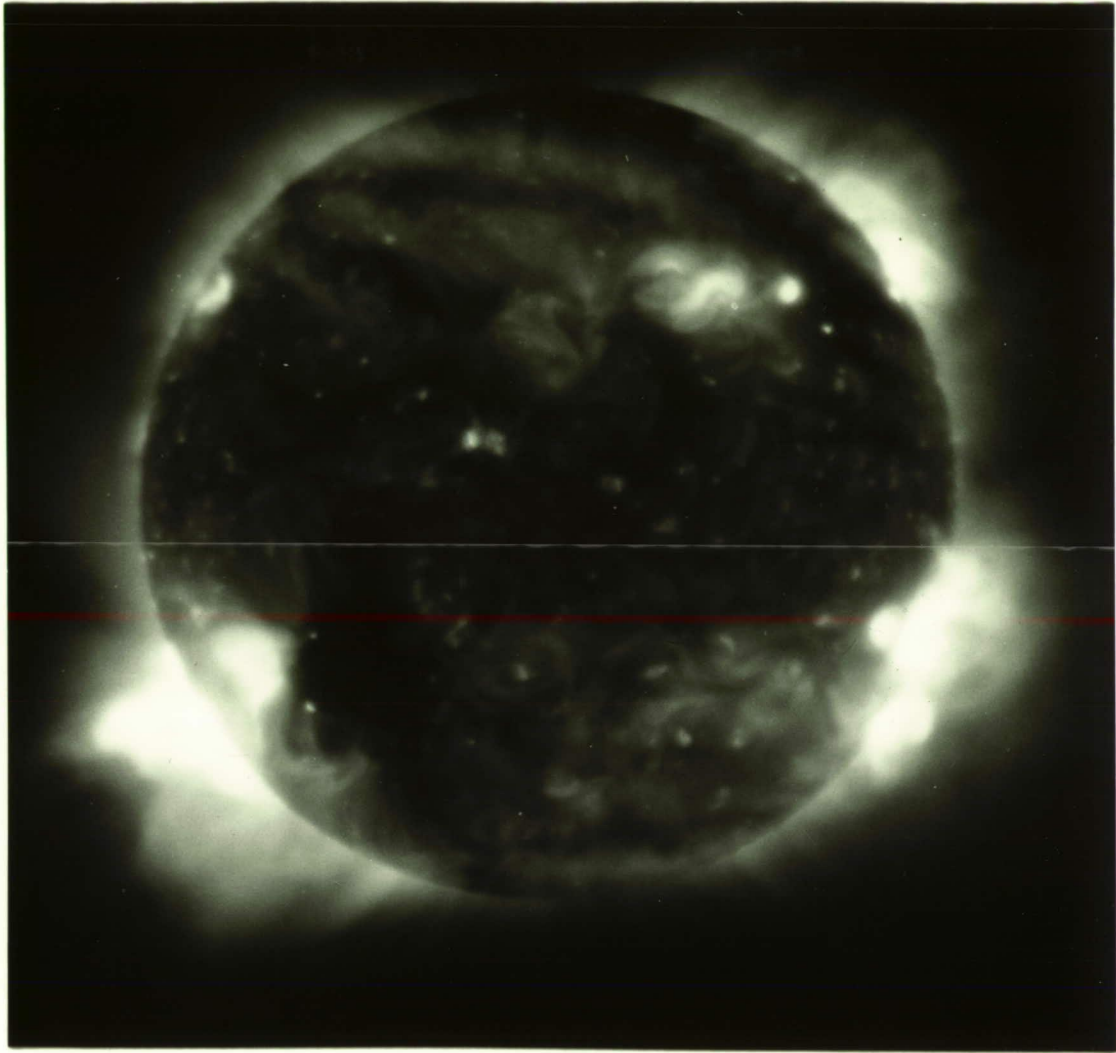
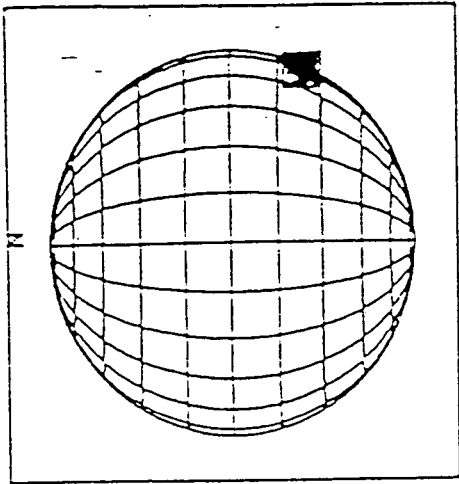
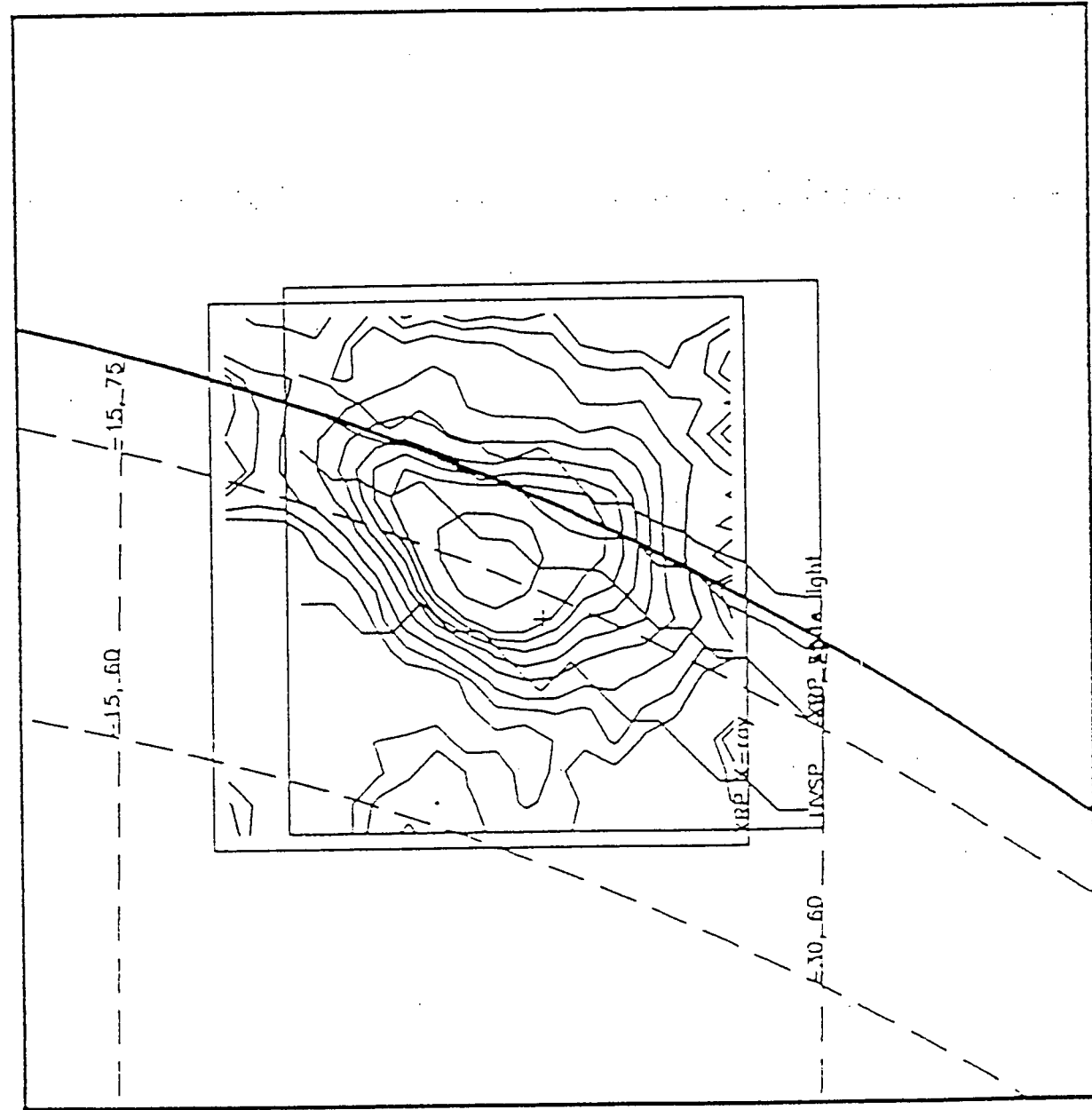


Figure 6



ORIGINAL PAGE
BLACK AND WHITE PHOTOGRAPH



XRP IMAGE

FCS Channel 1: NeIX

T: 87/346 18:16:17

Latitude : -22.43

Longitude: 74.40

Max cps = 89

Levels: 6,7,10,16,20,...700

AR 4901 in rocket

ghost map

Figure 7

Fe XVII

FSSxx1753.345 VOIGTF V3.7 09:06:33 31-MAR-88
START TIME: 18: 5:48.939 11/12/87
CHANNEL: 1 TIME PER STEP: 0.256 SEC SCAN: 1

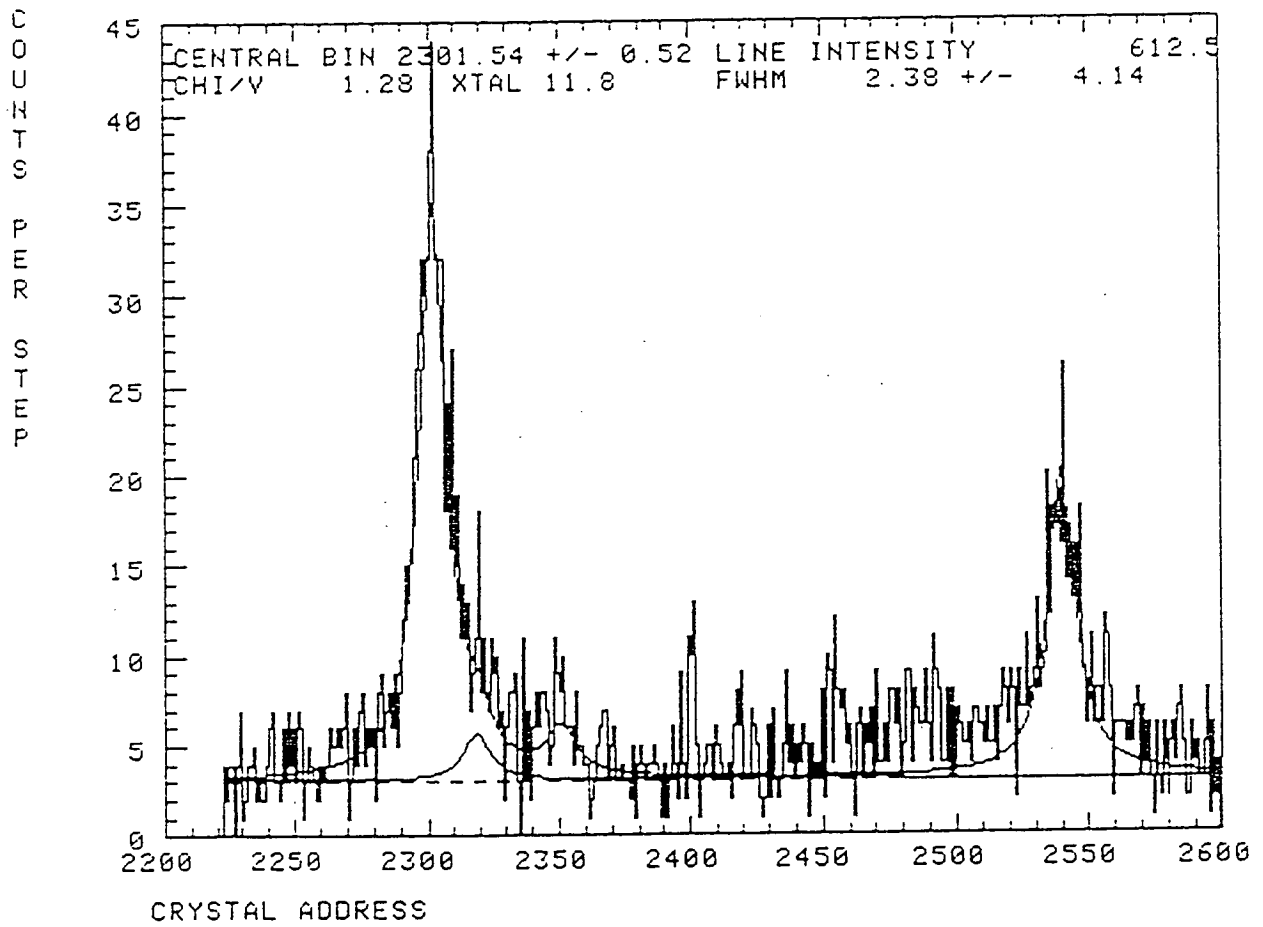


Figure 8

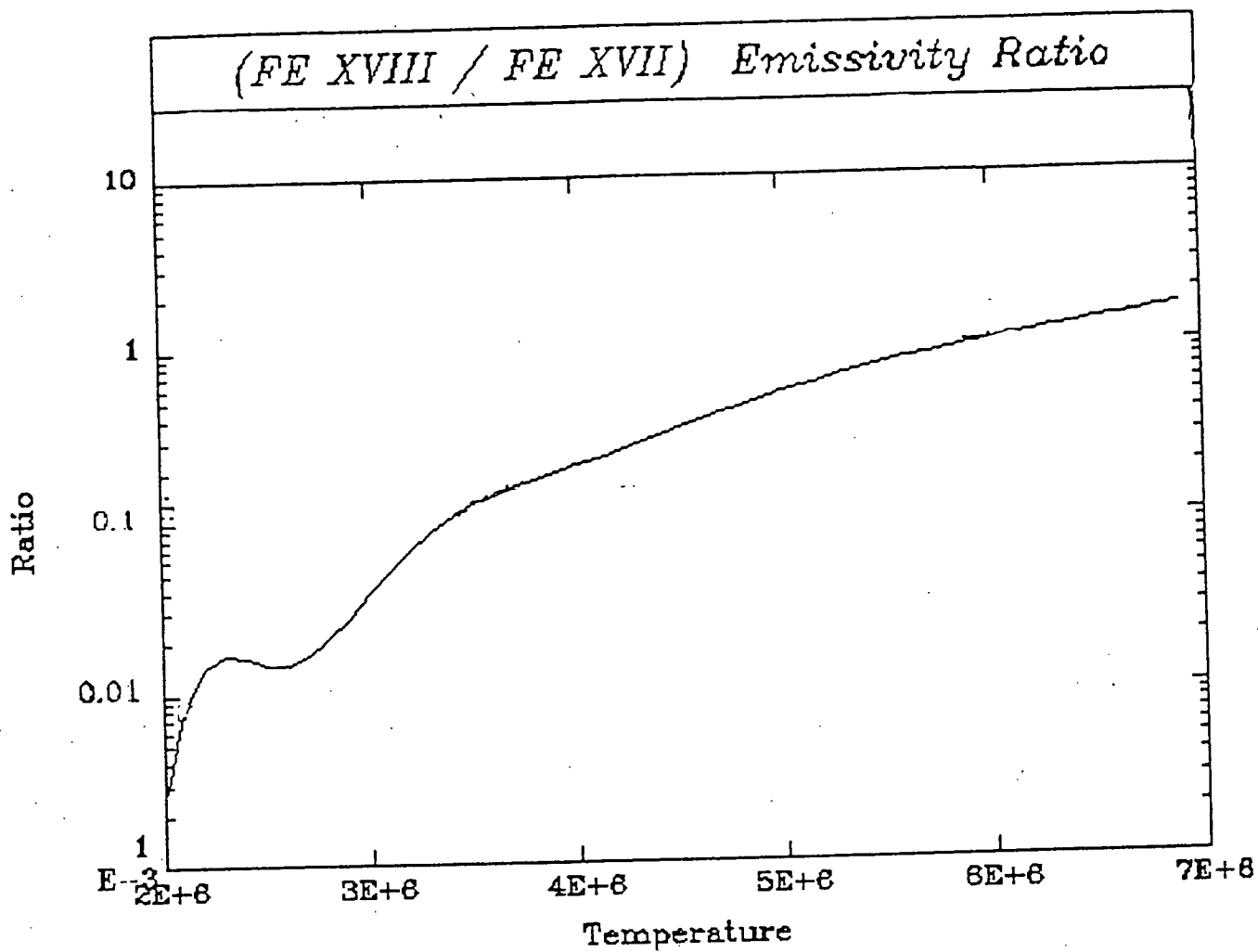


Figure 9

3. SCIENTIFIC PRESENTATIONS AND PUBLICATIONS

The results of the analyses performed in conjunction with contract NAS5-30141 have been presented to the scientific community as presentations at scientific meetings and workshops and as papers published in or submitted to the scientific literature. A list of the related publications is presented below followed by the abstract of a paper presented at an American Astronomical Society meeting. Appendix A is a paper submitted for publication in the Proceedings of the SPIE meeting in San Diego in August 1979.

3.1 List of Presentations and Papers

Moses, D., "AS&E Rocket Results," in CoMStOC Workshop Proceedings, ed. J.T. Schmelz, 1988, p. 37.

Moses, D. and Davis, J., "The Flight Test of a Grazing Incidence Relay Optics Telescope for Solar X-Ray Astronomy Utilizing a Thinned, Back-Illuminated CCD Detector," SPIE 982, 22, 1988.

Moses, J. and Davis, J., "Solar Cycle Variation of the X-Ray Bright Point Population: New Observations," Bull. AAS 20, 1008, 1988.

Moses, D. et al., "Correspondence between Solar Fine-Scale Structures in the Corona, Transition Region, and Lower Atmosphere from Collaborative Observations," Astrophys. J. (in preparation), 1989.

Moses, D., Schueller, R., Waljeski, K., and Davis, J., "Advances in Photographic X-Ray Imaging for Solar Astronomy," SPIE 1159, (in press), 1989.

Waljeski, K., Moses, J., Saba, J., and Strong, K., "Comparison of Soft X-Ray Broadband and Emission Line Temperature Diagnostics for Active Region Loops in the Solar Corona," Bull. AAS, 20, 1029, 1988.

Waljeski, K. and Moses, D., "Progress in Comparison of Broadband and Line Solar X-Ray Spectroscopy," presented at the Second Workshop on Thermal-Non-Thermal Interactions in Solar Flares, held at the University of Oxford, England, April 10-14, 1989.

Waljeski, K., Moses, J., Saba, J., Schmelz, J., and Webb, D., "Comparison of Soft X-Ray Broadband and Emission Line Plasma Diagnostics of Coronal Active Region Loops," Astrophys. J. (in preparation), 1989.

Webb, D. and Moses, D., "The Correspondence between Small-Scale Coronal Structures and the Evolving Solar Magnetic Field," Adv. Space Res. (in press), 1989.

3.2 Abstracts of Presentations

Bull. AAS 20, 1029, 1988

Comparison of Soft X-Ray Broadband and Emission Line
Temperature Diagnostics for Active Region Loops in the
Solar Corona

K. Waljeski (Brandeis University), J.D. Moses (American Science and Engineering, Inc.), J.R.L. Saba and K.T. Strong (Lockheed Palo Alto Research Laboratory)

Simultaneous observations of solar active region AR 4901 were made on 11 December 1987 by the Solar Maximum Mission X-Ray Polychromator and the AS&E Soft X-Ray High Resolution Imaging Sounding Rocket Payload. From these observations, a comparison is made of coronal plasma temperature diagnostics by two techniques: (1) broadband X-ray spectroscopy and (2) emission-line X-ray spectroscopy. A first order comparison is made assuming that the plasma in the emitting region is isothermal. The line intensity ratios of Fe XVII:Fe XVIII, Fe XVII:Mg XI, O VIII:Ne IX, Mg XI:Ne IX, O VIII:Fe XVIII, Mg XI:Fe XVIII, and Fe XVIII:Ne IX are used as temperature diagnostics for the line spectra. The ratio of the energy flux through an organic filter and a beryllium filter is used as a temperature diagnostic for the broadband images.

3.3 Scientific Papers

- 3.3.1 "Advances in Photographic X-Ray Imaging for Solar Astronomy"
Moses, D., Schueller, R., Waljeski, K., and Davis, J.

[See attached copy of paper.]



**American Science
and Engineering, Inc.**

Fort Washington
Cambridge, Massachusetts 02139
617-868-1600 Telex 921-458

SEPTEMBER 1989

ASE-5575

ADVANCES IN PHOTOGRAPHIC X-RAY IMAGING FOR SOLAR ASTRONOMY

BY:

D. MOSES, R. SCHUELLER, K. WALJESKI AND J.M. DAVIS

REPRINT OF PAPER, [1159-60]

PREPARED FOR:

**AUGUST 1989 MEETING OF SPIE IN SAN DIEGO, CALIFORNIA:
EUV, X-RAY AND GAMMA-RAY INSTRUMENTATION FOR ASTRONOMY
AND ATOMIC PHYSICS**

ADVANCES IN PHOTOGRAPHIC X-RAY IMAGING FOR SOLAR ASTRONOMY

D. Moses and R. Schueller
American Science and Engineering, Inc.
Cambridge, Massachusetts 02139

K. Waljeski
Brandeis University
Waltham, Massachusetts 02254

and

J.M. Davis
NASA, Marshall Space Flight Center
Huntsville, Alabama 35812

ABSTRACT

The technique of obtaining quantitative data from high resolution soft X-ray photographic images produced by grazing incidence optics was successfully developed to a high degree during the AS&E Solar Research Sounding Rocket Program and the S-054 X-Ray Spectrographic Telescope Experiment Program on Skylab. Continued use of soft X-ray photographic imaging in sounding rocket flights of the AS&E High Resolution Solar Soft X-Ray Imaging Payload has provided opportunities to further develop these techniques. The developments discussed include: (1) The calibration and use of an inexpensive, commercially available microprocessor controlled drum type film processor for photometric film development. (2) The use of Kodak Technical Pan 2415 film and Kodak SO-253 High Speed Holographic film for improved resolution. (3) The application of a technique described by Cook, Ewing, and Sutton⁽¹⁾ for determining the film characteristics curves from density histograms of the flight film. Although the superior sensitivity, noise level, and linearity of microchannel plate and CCD detectors attracts the development efforts of many groups working in soft X-ray imaging, the high spatial resolution and dynamic range as well as the reliability and ease of application of photographic media assures the continued use of these techniques in solar X-ray astronomy observations.

1. INTRODUCTION

Photographic detection of X-rays has been an essential technique in the history of X-ray applications since the discovery of the phenomena. X-ray photography has been primarily used as a position sensing (imaging) technique with only qualitative information on dosimetry. However, when sufficient effort is devoted to calibration (in all its various aspects), quantitative measurements of total energy deposit on a photographic medium have been successfully made for many applications.

One particularly successful use of quantitative measurements from photographic X-ray images was developed for the AS&E Solar Research Sounding Rocket Program and the S-054 X-Ray Spectrographic Telescope Experiment Program on Skylab. The details of this approach have been described in a series of papers and presentations⁽²⁻⁵⁾. In these programs, images of the solar soft X-ray (3-60 Angstroms) corona were formed by grazing incidence optics with angular resolution ranging from 2-5 arc seconds. Since the plate scales for these telescopes range from 7 to 10 microns

per arc second, the plate scale of the detector must be of the order of 7 to 20 microns. Furthermore, it is quite common to observe coronal structures which vary by over three orders of magnitude in soft X-ray emission within a single image; flares can generate a dynamic range of 10^6 . At the time of the design of these instruments, photographic film was the only detector suitable for space flight that possessed the required combination of sensitivity, spatial resolution, and dynamic range. Even today, this combination of performance, when coupled with the refinements in technique which are described in this paper, makes photographic media a very attractive choice for quantitative soft X-ray imaging of the solar corona.

2. PHOTOMETRIC DEVELOPMENT PROCEDURE

A large immersion-type continuous flow film processor was designed and built for the Skylab S-054 film processing. This machine was capable of maintaining variations in a test sensitometric visible light exposure to within ± 0.03 diffuse density units throughout the D log E curve for the film type used in this investigation (Kodak SO-212). Furthermore, the gamma of the test D log E curve was held to 1.50 ± 0.06 . While this machine provided excellent results with the 1300-foot rolls of 70 mm Skylab film, it is poorly suited to the 25-foot rolls of 35 mm film from the sounding rocket investigations because of the differences in the width of film, the difficulties in splicing a sufficient length of leader for the large processor, and the degradation in the machine following long periods of disuse.

Two aspects of the SO-212 film used in both the Skylab and Sounding Rocket investigations complicate the search for alternative solutions to the problem of photometric film processing: (1) The film was manufactured with a 2.5 mil base instead of the standard 4 mil base to reduce the bulk of the film rolls, and (2) the film was manufactured without the usual 1 micron gelatin topcoat to minimize absorption of low energy X-rays. The thin film base makes for serious handling difficulty in a processing system, particularly in loading reels for hand development. The lack of a topcoat makes the film very sensitive to pressure-induced developable artifacts in the handling process. Furthermore, the lack of a topcoat makes the development of the film extremely sensitive to the local concentration of developer chemistry. This difficulty made it impossible to obtain uniform development across the film with any type of hand development attempted by these investigators.

Through the suggestion of R. Haggerty of Crimson Camera Company, Cambridge, Massachusetts, the film processing needs of the sounding rocket program were met by the use of a mass produced, microprocessor controlled film processor manufactured by King Concept Corporation of Minneapolis, Minnesota. The processor is designed around a horizontally positioned light-tight drum into which the reel mounted film is placed. Under microprocessor control, chemistry is introduced and evacuated on a one-shot basis, and agitation is obtained through rotation of the drum. The temperature of the chemistry is maintained within 0.2 degrees centigrade by a water jacket, and the air temperature is controlled in the chamber where the drum is mounted. Kodak HC110 developer was used because of the ease of adjusting and repeatably obtaining the desired dilution. The greatest difficulty in the entire procedure was loading the 25-foot lengths of thin base SO-212 film on the stainless steel reels. This was finally accomplished with a modification to the King Concept Corporation device for film loading and a very practiced hand. Particular care was also devoted to monitor the temperature soak of the process, to avoid contamination effects, and to properly mix and store solutions.

The performance of the processor was monitored through the use of the same visible light sensitometric exposures (step-wedge with density increments of 1.414) as used in the Skylab effort. Visible light exposures were chosen over X-ray exposures based on the issues of ease and repeatability of exposure. The calibration effort consisted of 38 test batches conducted over a three-month interval.

The gamma of the D log E curve was found to vary along the length of the film within a given batch by no more than 0.03 from the mean. The film development batch exhibiting the greatest variation from the target gamma of 1.50 had a gamma of 1.37 (a variation of 0.13), although typical variations from the target value were of the order of 0.05. The extreme variation was obtained during a run significantly separated in time from the previous batches, indicating the need for a calibration run immediately before any flight run to test for changes in chemistry strength, temperature drifts, etc.

Measurement of variations in density throughout the sensitometric step wedges was complicated by the combination of the density structure of the step wedge, the extreme sensitivity of SO-212 film to local chemistry variations, and the direction of flow of the chemistry during agitation. Since agitation was accomplished in the drum by continuous rotation, the chemistry flow was constant and unidirectional along the length of the film. The length of the sensitometric step wedge was such that it could only be oriented with step exposures either increasing or decreasing along the length of the film. Therefore, the "downstream" density steps were always exposed to developer which was partially exhausted by the upstream density steps. While this developer exhaustion effect was never detected between two successive step wedges, the effect was always apparent within an individual step wedge. If the orientation of the sensitometric exposure was such that the more heavily exposed steps were "upstream" in the flow of the developer, the densest steps would have higher values and the less dense steps would have lower values than the case in which the least exposed steps were oriented "upstream." The two D log E curves would cross in the transition between the shoulder and straight line region with the greatest differences being restricted to the shoulder region (thus minimizing differences in gamma).

The variables of developer dilution, temperature, rotational agitation speed, rotational agitation direction (cw vs. ccw), and development time were explored and adjusted -- within the constraint of the target gamma value of 1.5 -- to minimize the effects of the developer depletion along flow direction. The resulting optimal development parameters were found to be dilution D of HC110 at 20°C for 3.75 minutes with 60 RPM rotational speed and a flow direction opposite that of the standard process. Within a single roll of film, density variations of 0.03 were found between step wedges of similar orientation with respect to developer flow direction. For step wedges of opposite orientation, the straight line portions were found to differ by less than 0.06 density units within a given roll of film while individual steps in the shoulder region could differ by as much as 0.12 density units. The density variations from roll to roll are in proportion to the variations in gamma from roll to roll.

The actual effect of depletion along the developer flow for the flight images is much less than that implied by the sensitometric step wedge measurements for two reasons: (1) The flight exposures are chosen such that the density values in the region of interest are within the straight line portion of the D log E curve to

provide energy resolution. (2) The size of the solar image on the film is much smaller than the size of the sensitometric exposure (24 mm x 18 mm vs. 121 mm x 10 mm), thus requiring much less developer for equivalent exposures. Furthermore, the size of the most dense region in a solar image, the core of a solar active region, is of the order of 0.5 mm. Since the active region spatial scale is less than the spacing between successive layers of film in the development reel, one would expect the mixing of the solution on these scales to make local developer depletion negligible. This expectation is borne out in the analysis described in the fourth section of this paper, where a local variation of the shape of the D log E curve in the longer exposures would become apparent in comparison with the shorter exposures. No localized developer depletion effects have been found in any analysis of the flight images.

Even the worst case variations in the automated film processor performance are greatly superior to performance obtained by hand development of SO-212 film, where seemingly random localized variations in density are found of the order of 0.20 density units throughout most of the D log E curve. The new automated processor does not match the consistency of performance from roll to roll of film obtained with the Skylab effort, but since all the film from a flight is developed in one load, the roll to roll variations are not as important. The consistency of performance within a given development load of film is comparable between the new processor and the Skylab machine. With careful attention to the inclusion of calibration white light and the appropriate X-ray sensitometric step wedge exposures with the development of a roll of film, excellent photometric results are obtained with the new system.

3. PHOTOGRAPHIC MEDIA

In preparation for the S-054 X-Ray Spectrographic Telescope Skylab mission, a special order photographic film was procured from Eastman Kodak in 1973. This film, labeled SO-212, is a standard aerographic emulsion with panchromatic response and was obtained without a gelatin top coat to improve its soft X-ray sensitivity. This stock of SO-212 has been used as the primary detector of the AS&E X-ray Imaging Sounding Rocket Program since its manufacture. The large volume required for a minimum special order makes it impractical to consider the manufacture of another batch of SO-212 (or an improved special order film) for the sounding rocket program. However, the considerable stock (in sounding rocket terms) left over from the Skylab mission has been kept in refrigerated storage and, other than an increase in the base density level by 0.05 to 0.07 diffuse density units, retains the same level of X-ray performance to within the uncertainty of variations in film processing and X-ray sensitometry.

Two main drawbacks exist in the use of SO-212 in the X-ray imaging sounding rocket program. The first drawback is the difficulties in handling the film which are described above. The second drawback is the level of granularity of the emulsion and the ultimate spatial resolution of the film relative to the plate scale of the telescope. Visible light tests with fine grain film show that the X-ray rocket mirror possesses angular resolution slightly better than 1 arc second, while both visible light test and X-ray flight images on SO-212 demonstrate resolution of several arc seconds at best.⁽⁶⁾

Listed in Table 1 are the candidates we have considered as supplements to the SO-212 film in an attempt to improve spatial resolution and handling. The T-Max 100

film has been used in the sounding rocket flight of an XUV telescope by Hoover *et al.*⁽⁷⁾, but we have not tested it. The SO-253 High Speed Holographic film was tested by AS&E during a flight on 31 January 1978.⁽⁸⁾ The Technical Pan 2415 (TP2415) was tested by AS&E during a flight on 15 August 1987.

TABLE 1 - PHOTOGRAPHIC FILM COMPARISON
(Kodak Technical Data based on visible light performance)

<u>Film Designation</u>	<u>RMS Granularity</u>	<u>Resolution (lines/mm)</u>
* SO-253 High Speed Holographic	< 5	1250
* Technical Pan 2415	From < 5-8 depending on development	320
T-Max 100	8	160
SO-212 Special X-Ray Emulsion Manufactured for Skylab Mission	20	160

* Available only with gelatin top coat.

X-ray sensitometry was conducted for the films which were flown and the results are presented in Figure 1. The development parameters used in this comparison for all three films are those producing the desired speed and contrast for SO-212. It is possible to somewhat modify the characteristic curves of TP2415 and SO-253 through changes in development parameters to obtain a better suited response for a given application, but the baseline of X-ray performance in Figure 1 is useful for comparison purposes.

The X-ray sensitivity of photographic film is obviously inversely proportional to the grain size and resolution. It has not been practical at this point to obtain low energy (44 Angstrom) sensitometry of the ultra-high resolution SO-253 film because the response of this film requires a month-long exposure with our current apparatus. The effect of the top coat on the TP2415 appears to be minimal since there does not appear to be a great difference in the 8.3 Angstrom and 44 Angstrom performance relative to the SO-212 performance. Although a quantitative determination of the relative importance to soft X-ray photographic response of grain size and top coating must await parameterization of these results in terms of a model such as that of Henke *et al.*⁽⁹⁾, it is useful to speculate on this subject. In a film with a fine grain structure, the higher volume fraction of AgBr grains implies a photon will, on average, traverse a smaller path length of emulsion gelatin before absorption by a developable grain relative to a more coarse grain film. It seems reasonable that the disadvantage of a top coat is compensated for by the reduction in gelatin traversed by a photon in the emulsion of TP2415 in comparison to SO-212. Higher maximum density in the shoulder region is expected in the more densely packed fine grain films. At lower energies, the decrease in penetration depth may minimize this effect.

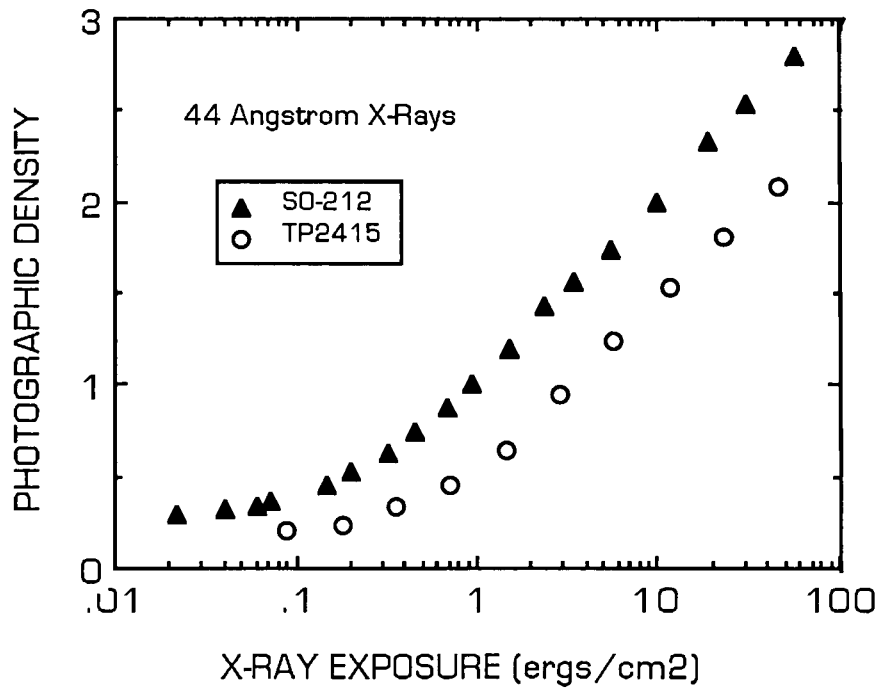
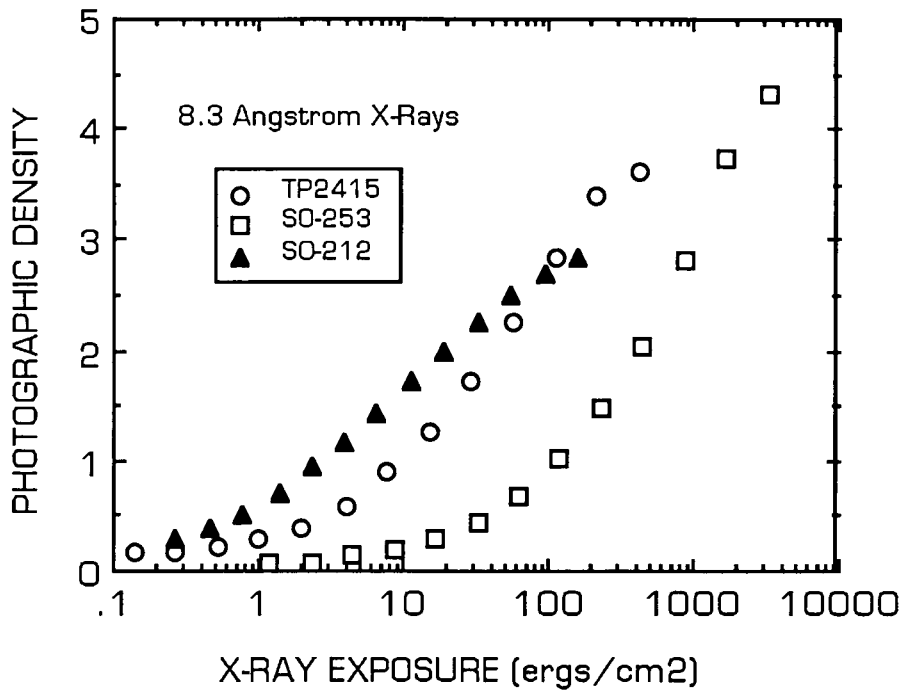


Figure 1. X-Ray Sensitometry of Photographic Film used in AS&E Solar Astronomy Soft X-Ray Imaging Sounding Rocket Program.

In practice, the target exposure times for SO-253 and TP2415 are increased relative to that of SO-212 by 5.5 and 2 stops, respectively. Since a typical sounding rocket flight provides about 5 minutes of observing time, the SO-253 is restricted to observations of bright active region cores and flares while the TP2415 can be used for everything but faint structures such as coronal holes and streamers. The SO-253 solar images show the active region cores resolved into loops in most regions with widths on the order of 1 arc second. The resolution of the TP2415 images fall midway between the resolution seen in the SO-253 images and that seen in the SO-212 images. The core regions which are resolved in the TP2415 images show complexes of loops with widths of 2 arc seconds.

An attempt is made to reproduce examples of these images in Figures 2 and 3. The limitations of photographic reproduction in these proceedings restricts the differences which can be shown. In Figure 2, a flaring bright point is clearly resolved into a loop like structure approximately 12 arc seconds long and 1 arc second wide in the SO-253 image of frame (c). The interpretation of this feature from the best SO-212 exposure in frame (b) would be that of a small linear region. It is impossible to identify any structure in the SO-212 image in frame (a) that was taken through the same filter as the SO-253 image of frame (c). In Figure 3, the differences between the TP2415 and the SO-212 are more subtle but still quite apparent in the original prints. The grain of the TP2415 is much finer than that of the SO-212, resulting in a higher confidence in the determination of the outline of these inherently diffuse structures. The arrow in frame (b) points to one of three small loops (approximately 2 arc-seconds wide and 8 arc-seconds long) in the southern boundary of Active Region 4839 that are resolved in the TP2415 images but not in the SO-212 images. The arrow in frame (d) points to the core loop system of the arcade of Active Region 4841 that is resolved into individual loops (approximately 2 arc-seconds wide and 1 arc-minute long) in the high temperature TP2415 image but is not resolved in the corresponding SO-212 image.

These results are very encouraging. Each of the three film types has a specific advantage that will be exploited in future flights. Because it is easy to compare the results from the very well calibrated SO-212 with the considerable archival X-ray coronal images, this film will remain the baseline film for the synoptic aspect of these investigations.

4. DETERMINATION OF THE FILM CHARACTERISTIC CURVE

Quantitative information about the properties of the coronal plasma can be obtained from soft X-ray solar images only if the film characteristic curve (i.e., the relationship between the photographic density of the image and the energy incident upon the film) is known. The determination of the applicable characteristic curve is significantly complicated by the fact that the film response is wavelength dependent and the wavelength distribution of the incident broadband spectrum through a given filter is not known a priori. Therefore, the determination of the film characteristics curve must be an iterative process. The wavelength dependence of the X-ray response of the SO-212 was determined through an exhaustive effort conducted during the S-054 Skylab Program^(3,4). The measured wavelength response of the film is combined (through a weighted average) with a model of the X-ray emission of a plasma with assumed temperature, density, ionization state, and composition (folded with the transmission function of the telescope and filter) to produce a modeled characteristic curve. This modeled curve must be compared with the photographic data from the flight in a convenient way, as the plasma parameters

Figure 2. Flaring Bright Point
photographed on
January 31, 1978.



(a)

WAVEBAND 8-39, 44-64Å
FILM S0-212
EXPOSURE 0.9 sec.



(b)

WAVEBAND 8-20Å
FILM S0-212
EXPOSURE 0.7 sec.



(c)

WAVEBAND 8-39, 44-64Å
FILM S0-253
EXPOSURE 20.3 sec.

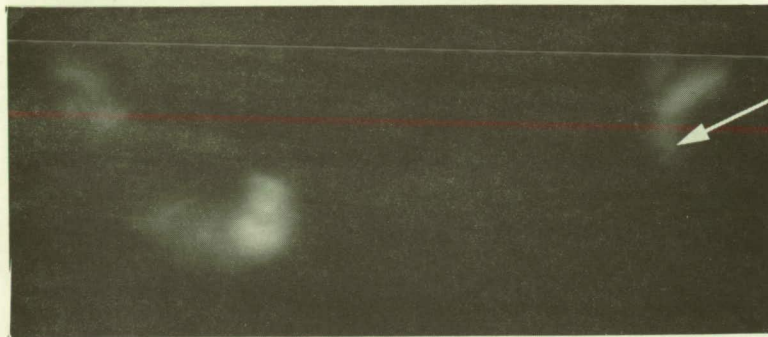
—|—|—
1 arc min.

Figure 3. Active Region complexes
4842, 4841, and 4839 in the
southern hemisphere on
August 15, 1987.



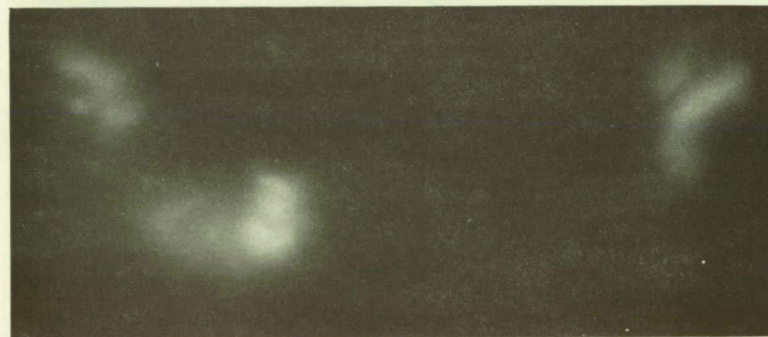
(a)

WAVEBAND 8-39, 44-60Å
FILM S0-212
EXPOSURE 3 sec.



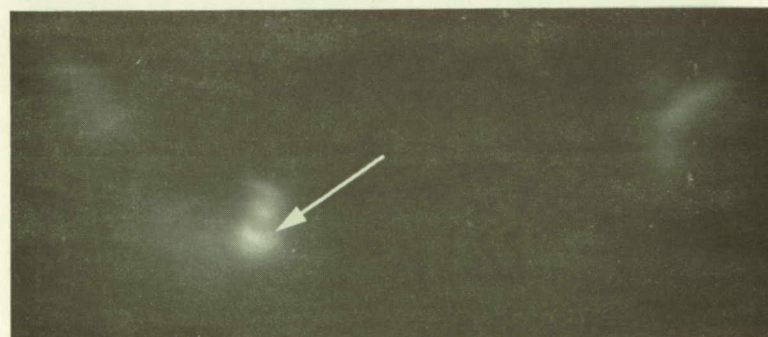
(b)

WAVEBAND 8-39, 44-60Å
FILM TP2415
EXPOSURE 9 sec.



(c)

WAVEBAND 8-20Å
FILM S0-212
EXPOSURE 9 sec.



(d)

WAVEBAND 8-20Å
FILM TP2415
EXPOSURE 20 sec.

5 arc min.

are iteratively adjusted to obtain a good fit to all the plasma diagnostics of these measurements.

For this discussion, we will use a parameterization of the film characteristic curve that was developed by VanSpeybroeck for the Skylab S-054 data analysis; it has been found to fit experimental film characteristic curves well. Other functional forms have been used to describe $D \log E$ curves (Tsubaki and Engvold⁽¹⁰⁾, Cook et al.⁽¹⁾); the VanSpeybroeck form is chosen for this analysis, as its parameters relate to quantities which can be easily measured from an experimental film characteristic curve. The VanSpeybroeck form of the relationship between the photographic density on the film is:

$$D = D_{base} + D_{max} + k \int_{a\mu E}^{\infty} \frac{e^{-z}}{z} dz - k \int_{a\mu E}^{\infty} \frac{e^{-z}}{z} dz e^{-D_{max}/k}$$

- where:
- D = net density on the film
 - E = power per unit area deposited on the film
 - D_{base} = density of the base fog level
 - D_{max} = maximum possible net density
 - au = film speed parameter, proportional to the reciprocal of the energy at which the density equals D_{base} in the extrapolation of the linear portion of the curve.
 - k = the slope of the linear portion of the $\ln E$ vs. D curve

The relationship between k (the slope of the characteristic curve expressed in terms of the natural logarithm of energy) and gamma (the slope of the characteristic curve expressed in the traditional terms of the logarithm base-ten of energy) is

$$\text{gamma} = 2.3 k$$

The four parameters of the characteristic curve to be determined are D_{base} , D_{max} , au, and gamma. D_{base} and D_{max} do not vary with wavelength, so these values can be measured in the laboratory. The other two parameters, au and gamma, are wavelength dependent and must be determined by an iterative technique.

Two methods of comparing a trial parameterized characteristic curve to the flight data have been utilized:

1. The scatter plot technique, which was developed as part of the Skylab ATM experiment data analysis of broadband soft X-ray images of the solar corona.
2. The density histogram technique, which was developed by Cook, Ewing, and Sutton⁽¹⁾ for the analysis of UV photographic spectra of the Sun.

By both of these techniques, the energy calibration is an iterative process between the laboratory calibration of the film and the flight data: The D-to-E calibration curve measured in the lab from a stepwedge, generated with monochromatic X-rays of a wavelength approximating the mean of the bandpass of the relevant filter, is used as a first approximation to the film characteristic curve. This approximation is refined iteratively by comparing image with different exposure times. The scatter plot and density histogram techniques differ in the methods used for image comparison.

The Scatter Plot Technique

By this technique, two digitalized images of differing exposure are, pixel by pixel, transformed and compared to determine the energy calibration curve. The images used must be co-aligned images of the same region, taken close enough together in time that the region can be assumed not to have changed between exposures. The trial $D \log E$ curve, taken from the monochromatic stepwedge, is used to convert the photographic densities $(D_1)_i$ and $(D_2)_i$, of each pixel, i , from each of the two exposures to powers per unit area, $(E_1)_i$ and $(E_2)_i$. A "scatter plot" is constructed by plotting E_1 vs. $(t_2/t_1) E_2$, where (t_2/t_1) is the ratio of the exposure times. If the slope of the best fit straight line to the scatter plot is unity, the film characteristic curve is correct. If not, a_u and γ are varied. The procedure is then repeated until no improvement in the scatter plot can be made. Note that the accuracy of this method is critically dependent upon the distribution of the points within the scatter plot. Furthermore, the scatter plot provides little sensitivity to, and feedback for, the toe region of the characteristic curve.

The Density Histogram Technique

This technique is the application of a method described by Cook *et al.*⁽¹⁾ for determining the film characteristic curve by transforming and comparing density histograms from images of differing exposures. Histograms of density are constructed from at least two digitalized images of the same region of the Sun, taken with different exposure times. One of the exposures is chosen as the base exposure, and bin-by-bin the histograms for the other exposure times are constructed from the base using the trial $D \log E$ curve, obtained from a monochromatic stepwedge. These transformed histograms are compared to the actual histograms of the appropriate exposure. The parameters of the characteristic curve, a_u and γ , are varied iteratively until the best match is found between the transformed histograms and the actual histograms.

This technique was used to determine the characteristic curves for film from the 11 December 1987 AS&E sounding rocket flight. The monochromatic reference stepwedge for this film is shown in Figure 4. Also plotted in Figure 4, is the fit to the stepwedge data obtained with the density histogram technique, for which $D_{base} = 0.16$, $D_{max} = 3.35$, $a_u = 5.70$, and $\gamma = 0.89$. It is apparent in Figure 4 that the density histogram technique provides the means to determine an excellent fit to the data of the characteristic curve parameters. Presented in Figure 5 is the characteristic curve determined by the density histogram technique using 3 s, 9 s, and 30 s exposures through the 8-39, 44-64 Angstrom bandpass filter of Active Region 4901, obtained during the 11 December 1987 flight of the AS&E Solar Rocket Payload. Also plotted for comparison in Figure 5 are the values of the monochromatic reference stepwedge shown in Figure 4. The final values of the parameters of the flight data characteristic curve were: $D_{base} = 0.16$, $D_{max} = 3.35$, $a_u = 7.00$, and $\gamma = 0.91$.

Although a determination of the characteristic curve by the scatter plot technique has not yet been completed for the image of Active Region 4901, in the data analysis of previous flights of this payload, the values of a_u and γ determined by the scatter plot technique for the comparable flight data are on the order of 10 to 20 percent greater than those determined for the reference 44 Angstrom

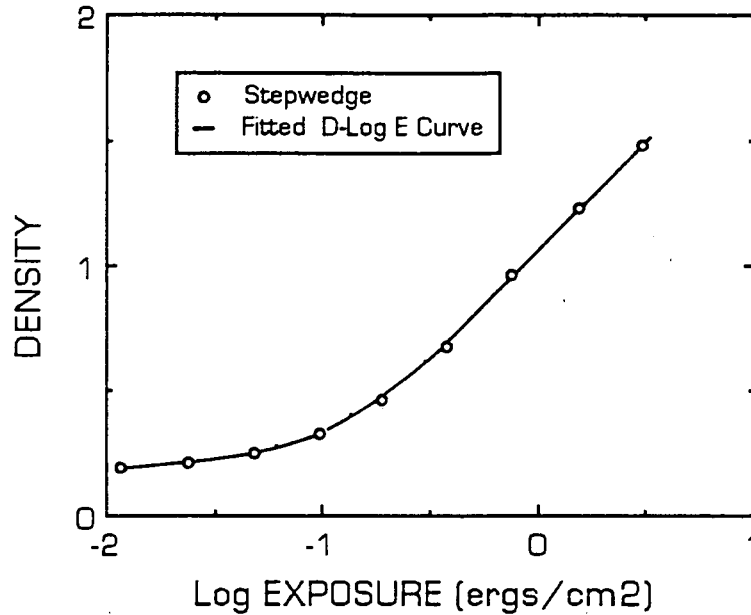


Figure 4. The 44 Angstrom monochromatic reference stepwedge for the 11 December 1987 rocket flight and the D log E curve fitted to this stepwedge data using the density histogram technique. ($D_{base} = 0.16$, $au = 5.70$, and $\gamma = 0.89$).

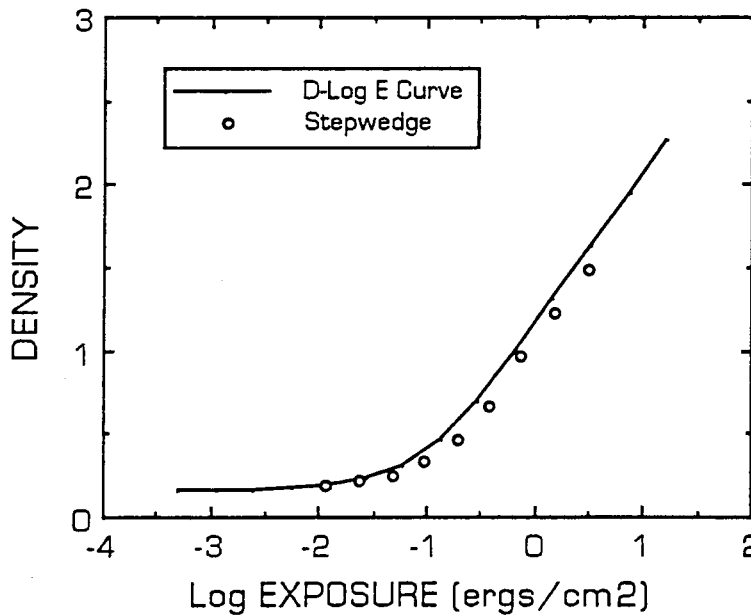


Figure 5. The characteristic curve for images from the 11 December 1987 rocket flight, as determined by the density histogram technique using 3 s, 9 s, and 30 s exposures through a polypropylene filter. ($D_{base} = 0.16$, $au = 7.00$, and $\gamma = 0.91$). The reference 44 Angstrom monochromatic stepwedge steps previously shown in Figure 4 are plotted again for comparison.

monochromatic stepwedge. Thus, both techniques find the same qualitative difference between the actual flight data and the reference monochromatic stepwedge data. As can be seen in Figure 5, making the assumption that the reference monochromatic stepwedge characteristic curve is equivalent to the flight data characteristic curve leads to an over-estimate of energy deposit in the focal plane by as much as 50 percent. The importance of this aspect of the image analysis is clear.

Discussion

The density histogram technique is expected to be the more reliable method of energy calibration for the following reasons:

1. The accuracy of the image co-alignment is less critical in the statistical approach of the density histogram technique. The pixel-by-pixel comparison of the scatter plot technique requires more exact co-alignment of the images.
2. As many exposures as are available may be used simultaneously to determine the characteristic curve by the density histogram technique. The scatter plot technique can compare two exposures only.
3. The density histogram technique is much less sensitive to the distribution of density values within a given exposure, and works well in the toe region of the characteristic curve.
4. It is easier to identify and ignore dirt, scratches, background, etc in the density histograms than in scatter plots.

We are only in the initial stages of implementing the density histogram technique in the analysis of flight data. A parallel effort with the scatter plot technique is planned for comparison. The initial results of the density histogram technique are very encouraging.

5. CONCLUSION

Three improvements in photographic X-ray imaging techniques for solar astronomy have been presented. The testing and calibration of a new film processor has been conducted, and the resulting product will allow photometric development of sounding rocket flight film immediately upon recovery at the missile range. Two fine-grained photographic films have been calibrated and flight tested to provide alternative detector choices when the need for high resolution is greater than the need for high sensitivity. An analysis technique used to obtain the characteristic curve directly from photographs of UV solar spectra has been applied to the analysis of soft X-ray photographic images, and the resulting procedure provides a more complete and straightforward determination of the parameters describing the X-ray characteristic curve than previous techniques. These improvements fall into the category of refinements instead of revolutions, indicating the fundamental suitability of the photographic process for X-ray imaging in solar astronomy. Although development of electronic detectors is the central component of our on-going development effort, photographic media will continue to be our baseline director for the near future.

6. ACKNOWLEDGEMENTS

We would like to acknowledge the crucial assistance and guidance of Robert Haggerty during all aspects of photometric film development in the AS&E Solar Physics Program. Anna Franco and Daniel O'Mara provided significant laboratory support to this project. We would like to thank S. Kahler, A. Krieger and D. Webb for useful discussions. This work builds on the strong tradition of quantitative image analysis that is a hallmark of AS&E. This work was supported by NASA contract NAS5-25496 and NASA GSRP Grant NGT-50308.

7. REFERENCES

1. Cook, J.W., Ewing, J.A., and Sutton, C.S., Pub. Astro. Soc. of the Pacific 100, 402, 1988.
2. Vaiana, G.S. VanSpeybroeck, L., Zombeck, M., Krieger, A.S., Silk, J.K., and Timothy, A.F., Space Sci. Inst. 3, 19, 1977.
3. Haggerty, R., Simon, R., Golub, L., Silk, J.K., Timothy, A.F., Krieger, A.S., and Vaiana, G.S., AAS Photo. Bull. 10, 8, 1975.
4. Simon, R., Haggerty, R., Golub, L., Krieger, A.S., Silk, J.K., and Timothy, A.F., Presented at the AAS Working Group on Photographic Materials, Rochester, NY, August 1974.
5. Krieger, A.S., SPIE, 106, 24, 1977.
6. Davis, J.M., Krieger, A.S., Silk, J.K., and Chase R.C., SPIE 184, 96, 1979.
7. Hoover, R.B., Barbee, T.W., Lindblom, J.F., and Walker, A.B.C., Kodak Tech Bits, pp. 1-6, June 1988.
8. Davis, J.M., Quarterly Progress Report No. 11, Contract NAS2-8683, 1977.
9. Henke, B.L., Kwok, S.L., Uejio, J.Y., Yamada, H.T., and Young, G.C., J. Opt. Soc. Am. B 1, 818, 1984.
10. Tsubaki, T. and Engvold, O., AAS Photo-Bulletin 9, 17, 1975.

APPENDIX A

CoMStOC: Coronal Magnetic Structures Observing Campaign

CoMStOC:
Coronal Magnetic Structures Observing Campaign

The Coronal Magnetic Structures Observing Campaign is a program of coordinated observations of active regions on the Sun. The purpose of the campaign is to obtain and use coordinated soft X-ray, microwave, and related observations (H α , magnetographs, UV, etc.) of coronal magnetic structures, both quiescent active region and pre- and post-flare loops, to deduce the quantitative magnetic and plasma properties of these structures. The program is especially designed to maximize scientific return from the Solar Maximum Mission's Soft X-Ray Polychromator (XRP) and the VLA. The campaign will occur primarily during the period November 1987 - March 1988, when the VLA is in B or C configuration, for maximum spatial and spectral coverage at microwave frequencies of structures in the lower corona and upper transition zone.

The observations will be done in conjunction with theoretical modeling of the microwave and soft X-ray emissions from magnetic loops. Comparing the coordinated observations with computations of the emission from loop models can yield reliable quantitative information about the magnetic and thermal properties of structures in the solar corona and transition zone. An important aspect of this work is the ability to deduce the strength and structure of the magnetic field in the corona and transition zone, in addition to plasma temperatures and densities. The microwave observations provide the only way of measuring magnetic field strengths in the solar corona. Unlike photospheric magnetograms, which measure the longitudinal component of the photospheric magnetic field, the microwave observations can provide a measure of the total magnetic field strength in the corona. This information is of fundamental importance for understanding coronal heating and flares, since both are intimately associated with coronal magnetic fields, as well as for understanding the origin and evolution of coronal magnetic fields.

Single-frequency microwave observations do not generally lead to unambiguous determinations of coronal magnetic field strengths, since two different mechanisms, thermal bremsstrahlung (free-free) and thermal gyroresonance (cyclotron) emission, and possibly nonthermal gyrosynchrotron radiation, can contribute to the emission. The coordinated soft X-ray observations are important for sorting out the microwave emission mechanism and learning more about the thermal and spatial properties of the coronal plasma. Multi-frequency, high spatial resolution microwave observations of total intensity and circular polarization are also important for sorting out the emission mechanism, determining the cyclotron harmonic when the emission is gyroresonance, and deducing the physical properties of the magnetic structures as a function of height in the solar atmosphere. Observations with the VLA at multiple frequencies around 1.5 GHz and 5 GHz are particularly desirable for this. Coordinated observations with the Owens Valley frequency-agile interferometer are also highly desirable.

In addition to the soft X-ray and microwave observations, H α images, magnetograms, and related ground-based observations will always be solicited. These are important for comparison with the microwave and soft X-ray data. Of special interest is coordinated observations with the new vector magnetographs. Coronal fields theoretically extrapolated from the magnetograph observations can be compared with the results deduced from the X-ray and microwave observations.

LIMITED REPRODUCIBILITY

**MORE THAN 20% OF THIS
DOCUMENT MAY BE
AFFECTED BY:**

- FAINT OR BROKEN TYPE**
- COLOR PHOTOGRAPHS**
- BLACK AND WHITE PHOTOGRAPHS**
- FOLDOUTS**
- DOT MATRIX PRINT**
- CHARTS/GRAPHS with SCRIPT NOTATION**
- NON-ROMAN ALPHABET**
- OTHER (specify)_____**